GL00418

FC
USGS
OFR
80-1163

A Magnetotelluric Survey of the San Francisco Volcanic Field, Arizona

By

R. H. Ware

(Cooperative Institute for Research in Environmental Sciences)
University of Colorado/NOAA
Boulder, CO 80309

and

J. E. O'Donnell

Open-File Report 80-1163

1980

This report is preliminary and has not been reviewed or edited for conformity with U.S. Geological Survey standards or nomenclature.

Introduction

In September 1979, the Cooperative Institute for Research in Environmental Sciences (CIRES) in cooperation with the USGS made 17 magnetotelluric (MT) soundings in the San Francisco Volcanic Field near Flagstaff, Ariz. These soundings complement aeromagnetic (Sauck and Sumner, 1970), gravity (J. D. Hendricks, unpublished data, 1971), and seismic surveys of the area. This work was stimulated by interest in the volcanic field as a potential hot, dry rock geothermal energy site (Wolfe et al, 1975).

Figure 1 shows the location of the MT sites in respect to the prominent features of the San Francisco Volcanic Field. Also shown are plots of resistivity versus depth, which are inverted from the apparent resistivity curves, and well locations, which have resistivity logs. The coordinates of the wells and MT sites are listed in table 1.

The well logs provide an independent check of resistivity values at depths near 1.5 km. Specifically, near 1.5 km in depth, resistivities are 1000 ±100 Ω-m (MT) and 850 ± 200 Ω-m (well logs). Errors were estimated from scatter in both cases. The averaged well-log plot of resistivity versus depth is included at the end of appendix B. Well resistivity logs were provided by the USGS, Flagstaff.

Data Collection

The USGS real-time five-component MT system operating in the frequency range of about 0.004 to 20 Hz was used to collect the data (Stanley and Frederick, 1979). Successful operation of the MT system was largely a result of the technical expertise of Dick Sneddon, USGS. Jim Demay also assisted with the general management of the field experiments.

Earth response functions derived from the real-time data analysis are shown in appendix A. Plotted as a function of frequency are:

a) apparent resistivity amplitude,

b) apparent resistivity phase,

c) principal axis angle, and

d) tipper angle.

Data evaluation

Data reliability was evaluated using the product of the multiple and partial coherences calculated by the real-time system. Data were not used if the coherence product were less than 0.80. The real time system uses time series of 128 points and also decimates the series to increase the digitizing interval. The time series is low pass filtered and the spectra are stacked to improve the signal to noise ratio. Also shown in appendix A are solid lines which were fitted by hand to the principal, apparent resistivity values R_{xy} and R_{yx}. The dotted line is the geometric mean $\sqrt{R_{xy} R_{yx}}$ and is included to provide a one-dimensional view of the resistivity soundings. Slopes were constrained to less than $\pm 45^{o}$, which is required for one- or two-dimensional modeling. The curves were then inverted using a continuous inversion algorithm (Bostick, 1977). The inverted curves which plot resistivity versus depth are included in appendix B.

A regional view of the resistivity soundings is shown in figure 1. Details of a sounding at a particular site may, of course, be viewed in the full-size inversion in appendix B. The inversion of MT data recorded near two- and, particularly, three-dimensional structures does not necessarily result in a unique sounding curve (Berdichevsky and Dmitriev, 1976). In particular, lateral changes in resistivity at depths less than 2 km can influence resistivity-depth inversions to depths greater than 20 km. Modeling of near-surface resistivity structures has demonstrated this (Morrison and Lee, 1979). A rather firm indication of lateral inhomogeneities is the separation or splitting of resistivity-depth curves derived from R_{xy} and R_{yx}.

Results

A detailed interpretation of the results is not presented here in order to make the data available as quickly as possible. However, several interesting aspects of the data will be mentioned briefly.

A consistent trend is noted in the angle of the principal axis. They are oriented from due north to 15°W at all sites and at essentially all frequencies measured. In addition, the maximum resistivity at most of the nine sites which show splitting is generally oriented parallel to the principal axis. At sites 12 and 14, R_{max} crosses over, but is parallel where there is substantial splitting. Only site 10 shows R_{max} perpendicular to the principal axis. The youngest volcanic vent in the area (Sunset Crater) is close to site 10 which, relative to all other sites, (1) has the most profound splitting and (2) has the lowest absolute resistivity value measured at any site.

Acknowledgments

The time and enthusiasm which was contributed by Dal Stanley, Ed Wolfe, and George Ulrich are greatfully acknowledged. This research was supported by USGS grant #14-08-0001-17874.

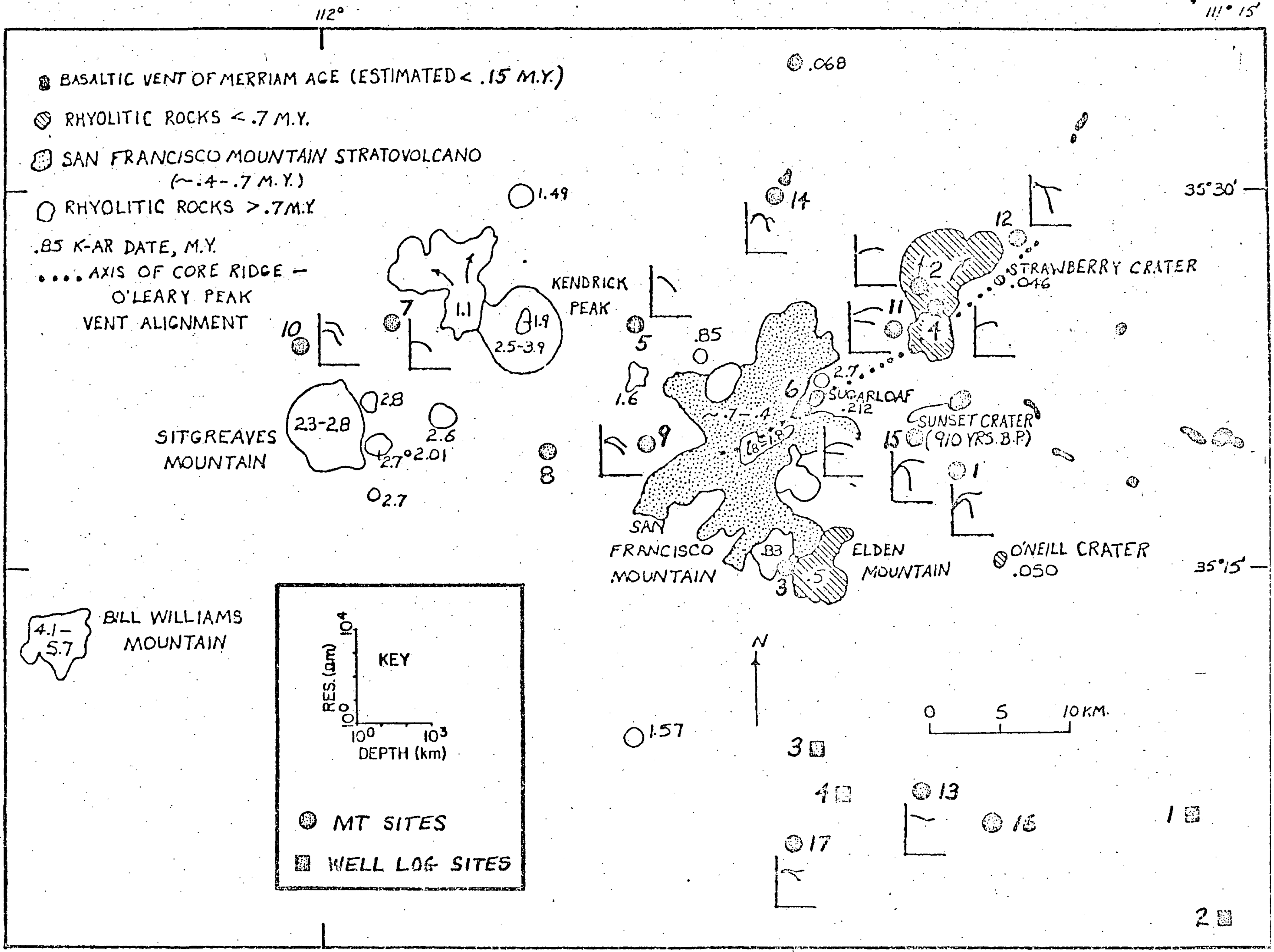

112°
111° 15'
35°30'
35°15'
BASALTIC VENT OF MERRIAM AGE (ESTIMATED < .15 M.Y.)
RHYOLITIC ROCKS < .7 M.Y.
SAN FRANCISCO MOUNTAIN STRATOVOLCANO (~.4-.7 M.Y.)
RHYOLITIC ROCKS > .7 M.Y.
.85 K-AR DATE, M.Y.
AXIS OF CORE RIDGE - O'LEARY PEAK VENT ALIGNMENT
KENDRICK PEAK
SITGREAVES MOUNTAIN
SAN FRANCISCO MOUNTAIN
ELDEN MOUNTAIN
STRAWBERRY CRATER
SUGARLOAF
SUNSET CRATER (910 YRS. B.P.)
O'NEILL CRATER
BILL WILLIAMS MOUNTAIN
.068
1.49
1.1
1.9
2.5-3.9
.85
1.6
2.7
.212
.046
.050
2.3-2.8
2.8
2.6
2.7
2.01
2.7
~.7-.4
.83
.5
4.1-5.7
1.57
N
0
5
10 KM.
KEY
RES. (Ωm)
10^0
10^4
10^0
10^3
DEPTH (km)
MT SITES
WELL LOG SITES

Table 1

COORDINATES OF MT SITES AND WELL RESISTIVITY LOG SITES

MT Sites	°N	°W
1. Cinder Lake	35.316	111.518
2. Water Tank	35.431	111.538
3. Dry Lake Hills	35.266	111.634
4. Dead Man Mesa	35.424	111.530
5. Kendrick Park	35.406	111.741
6. Lockett Meadow	35.359	111.619
7. Community Tank	35.405	111.926
8. Malpais Tank	35.332	111.815
9. Hart Prarie	35.342	111.732
10. Boulin Tank	35.381	112.042
11. O'Leary Peak	35.407	111.555
12. Dead Man Wash	35.478	111.431
13. Marshall Lake	35.113	111.538
14. Indian Flat	35.482	111.658
15. Lennox Crater	35.352	111.527
16. Prime Lake	35.097	111.531
17. Roadbed Tank	35.094	111.621

Well log sites

1.	35.090	111.309
2.	35.009	111.287
3.	35.133	111.604
4.	35.104	111.583

APPENDIX A

Earth response functions derived from real-time data analysis, plotted versus frequency. Top to bottom the plots show apparent resistivity amplitudes, apparent resistivity phase, and orientations of the principal axis and tipper.

APPENDIX B

Appendix B contains averaged well-log plots of resistivity versus depth, which are inverted from the apparent resistivity versus frequency curves, where R1 = R_{max}, R2 = R_{min}, and R3 = average of the apparent resistivity curves R_{max} and R_{min}.

REFERENCES

Berdichevsky, M. N. and V. I. Dmitriev, 1976, Basic principles of interpretation of magnetotelluric sounding curves, <u>in</u> KAPG Geophysical Monograph on Geoelectric and Geothermal Studies, Budapest, p. 165-221.

Bostick, F. X., 1977, A simple almost exact method of MT analysis, <u>in</u> Workshop on Electrical Methods in Geothermal Exploration, Jan. 1977, Proceedings: Univ. of Utah, Salt Lake City, p. 174-183.

Morrison, H. F., K. H. Lee, G. Opplinger and A. Day, 1979, Magnetotelluric studies in Grass Valley, Nevada, Lawrence Berkeley Laboratory, LBL-8646, ___p.

Sauck, W. A., and J. S. Sumner, 1970, Residual aeromagnetic map of Arizona: Dept. of Geosciences, Univ. of Arizona, Tucson, ___p.

Stanley, W. D. and N. V. Frederick, 1979, USGS real-time magnetotelluric system: USGS Open-file report, 79-R27, ___p.

Wolfe, E. W., G. E. Ulrich and R. B. Moore, 1975, San Francisco volcanic field-potential hot dry rock sites, Administrative report prepared at request of T. R. McGetchin, Los Alamos Scientific Laboratory, ___p.

Figure 1. Map showing distribution of ages of volcanic rocks in the San Francisco Volcanic Field (modified from Wolfe et al., 1975). Added to Wolfe's map are sites of well resistance logs, MT sites, and resistivity vs. depth plots. The coordinates of the sites are listed in table 1.

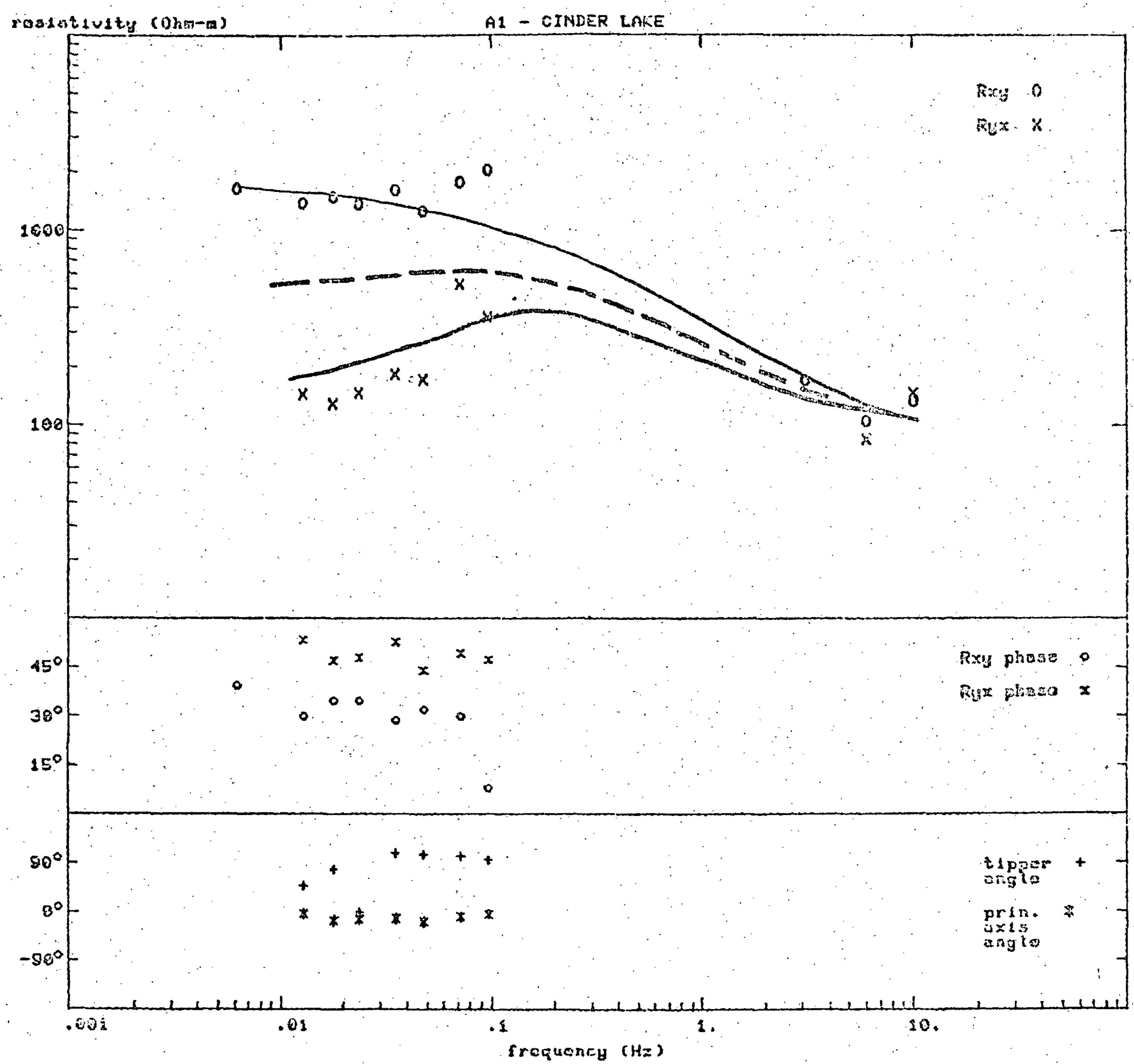

resistivity (Ohm-m)
A1 - CINDER LAKE
Rxy O
Ryx X
1000
100
Rxy phase o
Ryx phase x
45°
30°
15°
tipper angle +
prin. axis angle
90°
0°
-90°
.001
.01
.1
1.
10.
frequency (Hz)

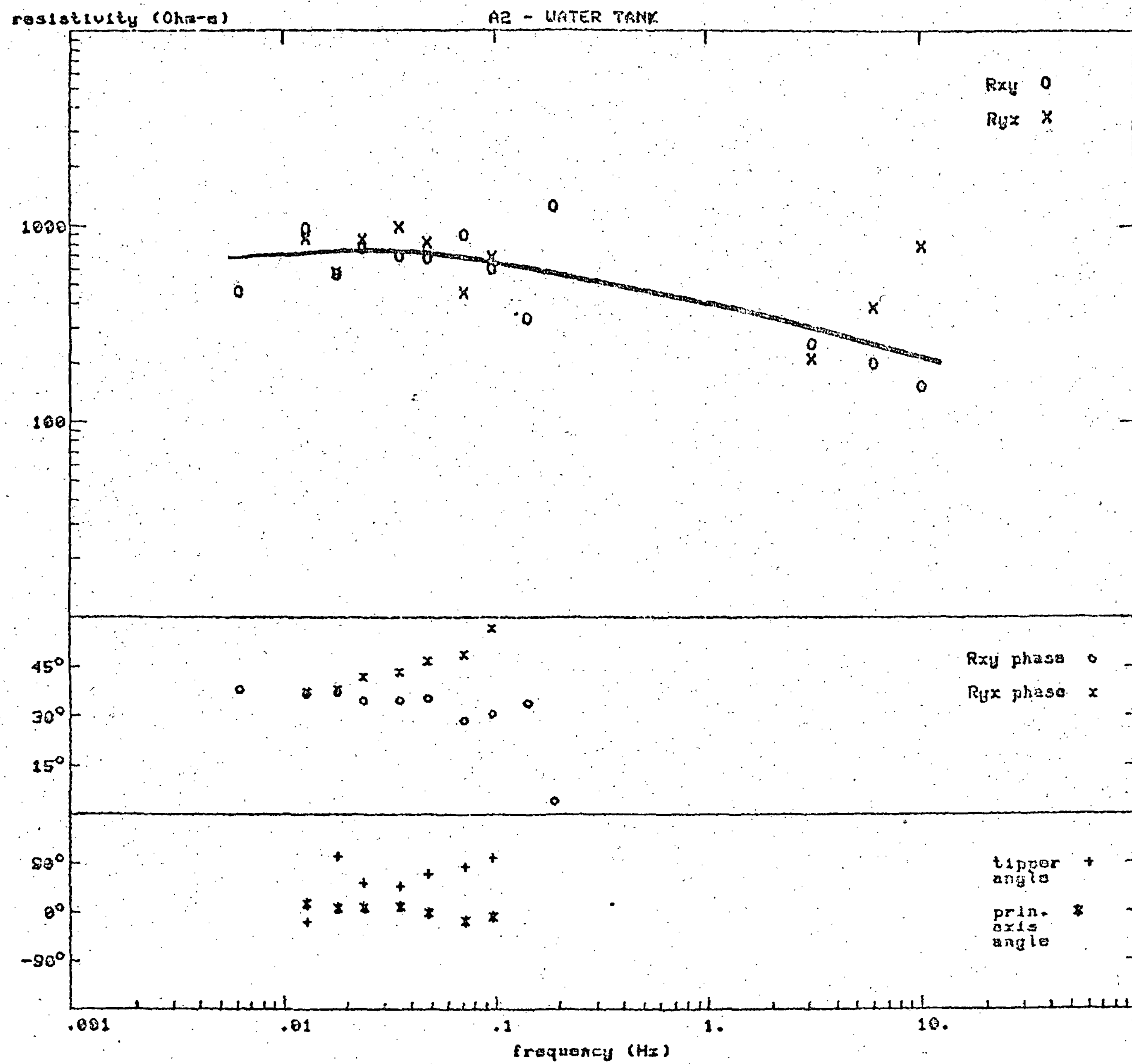

resistivity (Ohm-m)
A2 - WATER TANK
Rxy O
Ryx X
1000
100
Rxy phase o
Ryx phase x
45°
30°
15°
tipper angle +
prin. axis angle
90°
0°
-90°
.001
.01
.1
1.
10.
frequency (Hz)

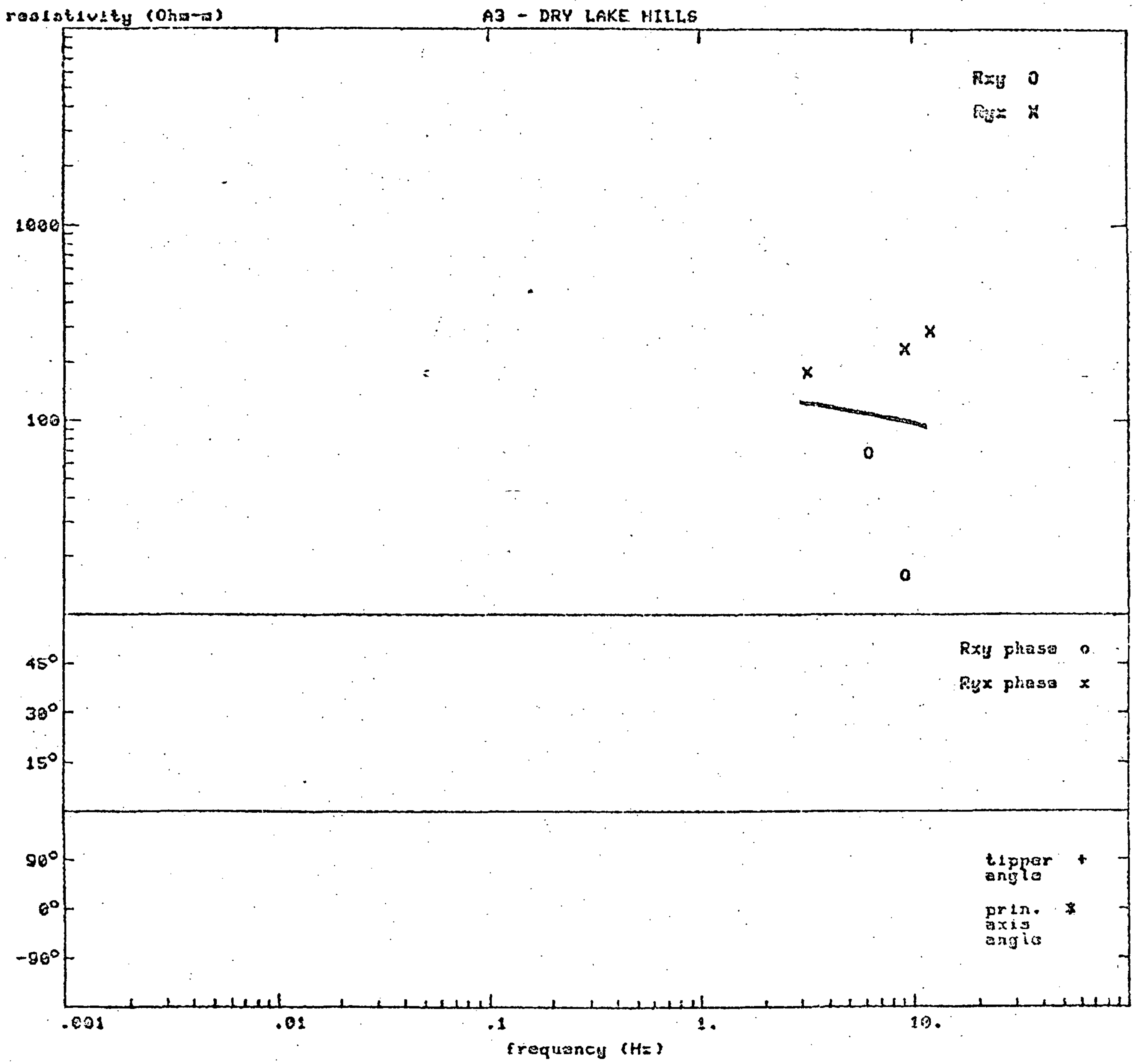
resistivity (Ohm-m)
A3 - DRY LAKE HILLS
Rxy O
Ryx X
1000
100
Rxy phase o
Ryx phase x
45°
30°
15°
tipper angle +
prin. axis angle *
90°
0°
-90°
.001
.01
.1
1.
10.
frequency (Hz)

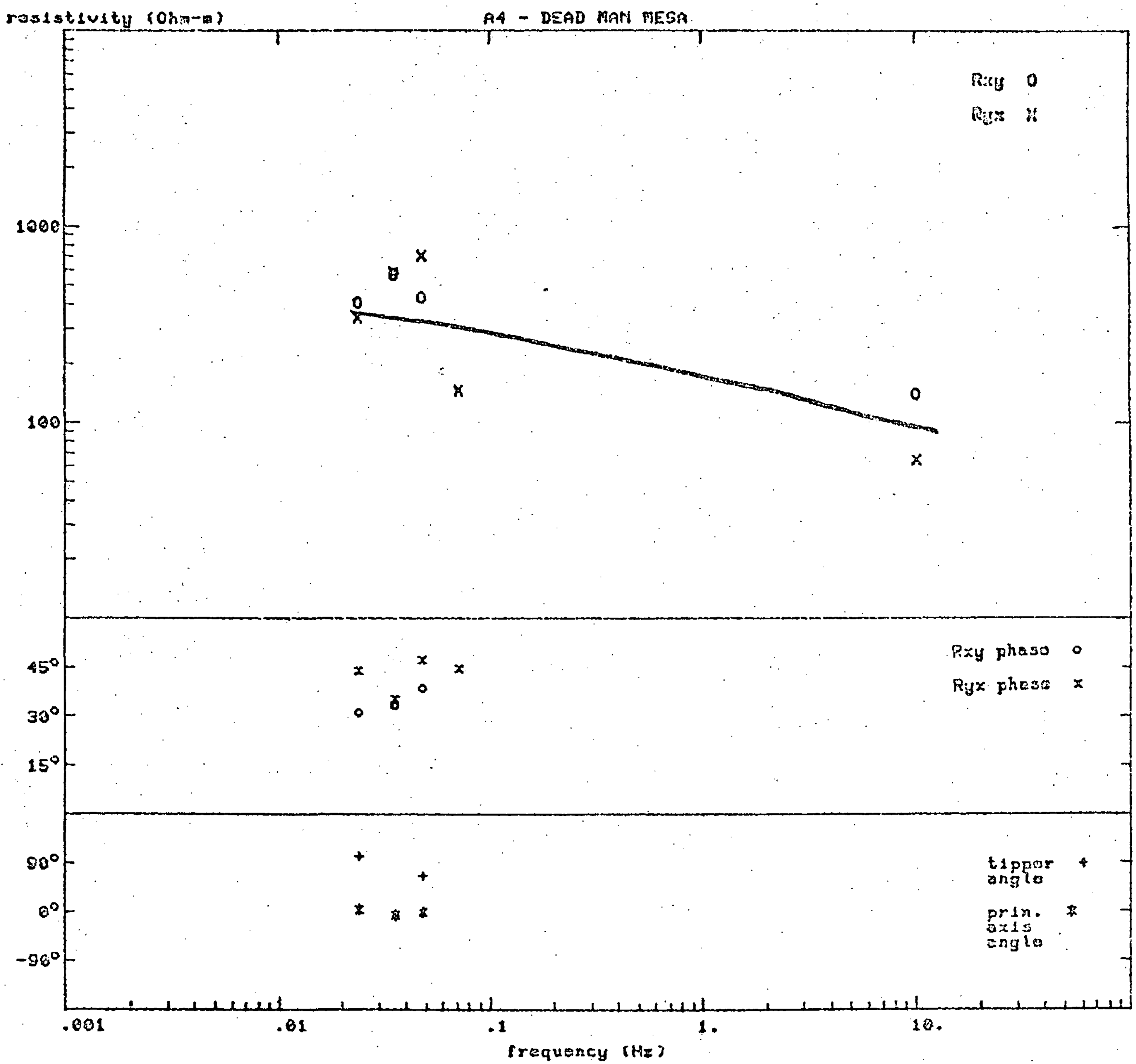

resistivity (Ohm-m)
A4 - DEAD MAN MESA
Rxy O
Ryx X
1000
100
Rxy phase o
Ryx phase x
45°
30°
15°
90°
0°
-90°
tipper angle +
prin. axis angle
.001
.01
.1
1.
10.
frequency (Hz)

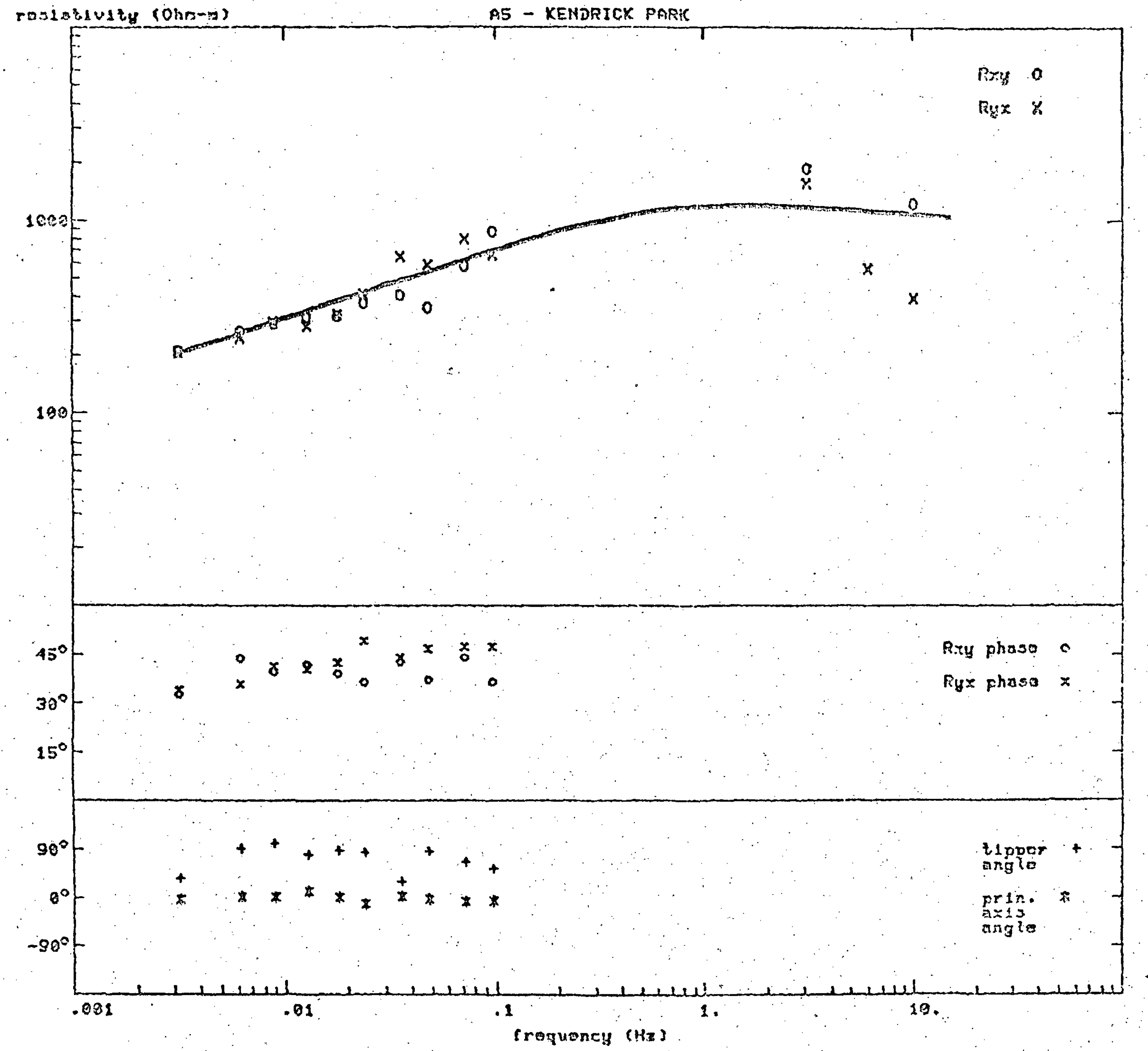

resistivity (Ohm-m)
A5 - KENDRICK PARK
Rxy O
Ryx X
1000
100
45°
30°
15°
Rxy phase o
Ryx phase x
90°
0°
-90°
tipper angle +
prin. axis angle
.001
.01
.1
1.
10.
frequency (Hz)

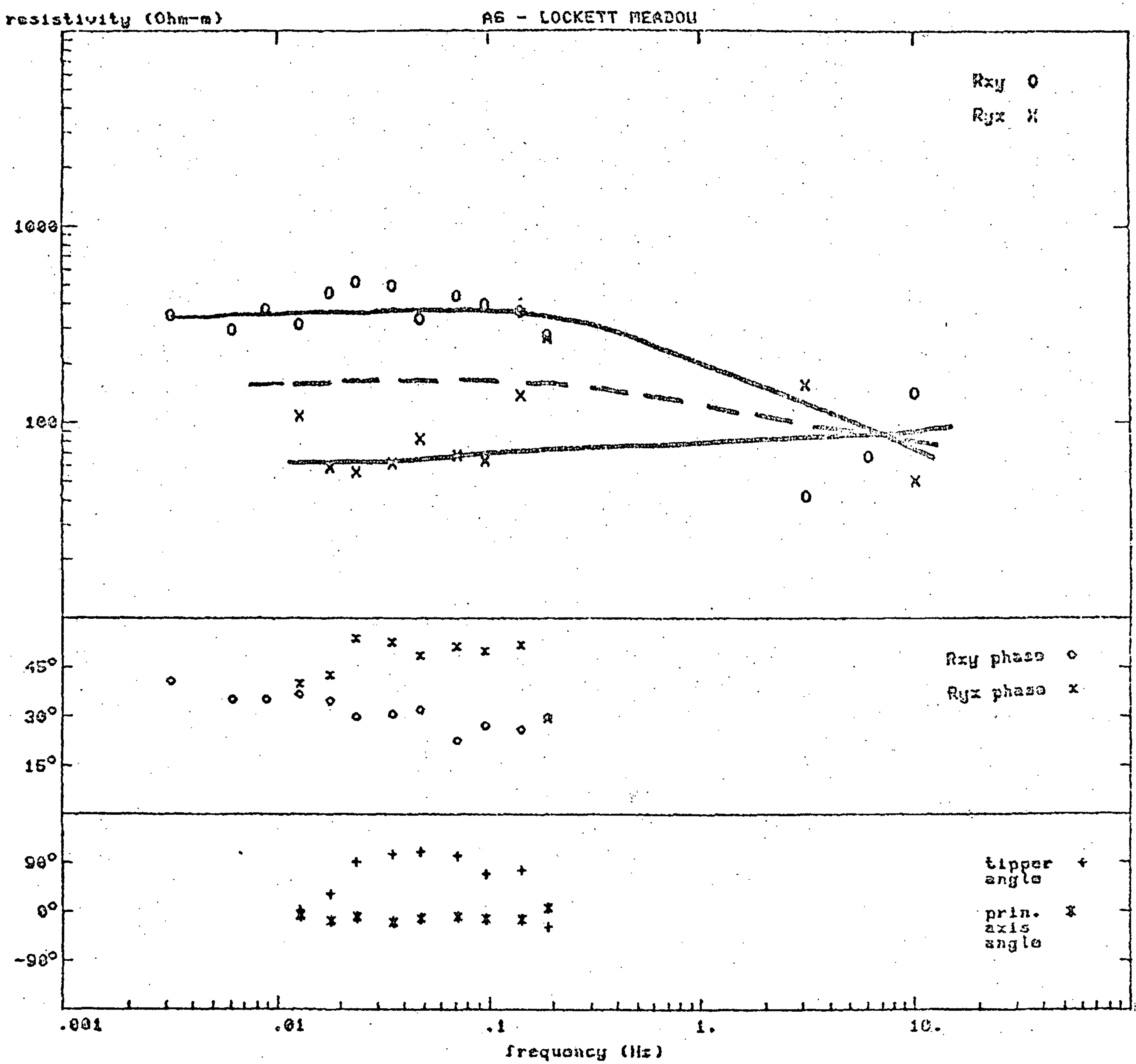
resistivity (Ohm-m)
A6 - LOCKETT MEADOW
Rxy O
Ryx X
1000
100
45°
30°
15°
Rxy phase o
Ryx phase x
90°
0°
-90°
tipper angle +
prin. axis angle *
.001
.01
.1
1.
10.
frequency (Hz)

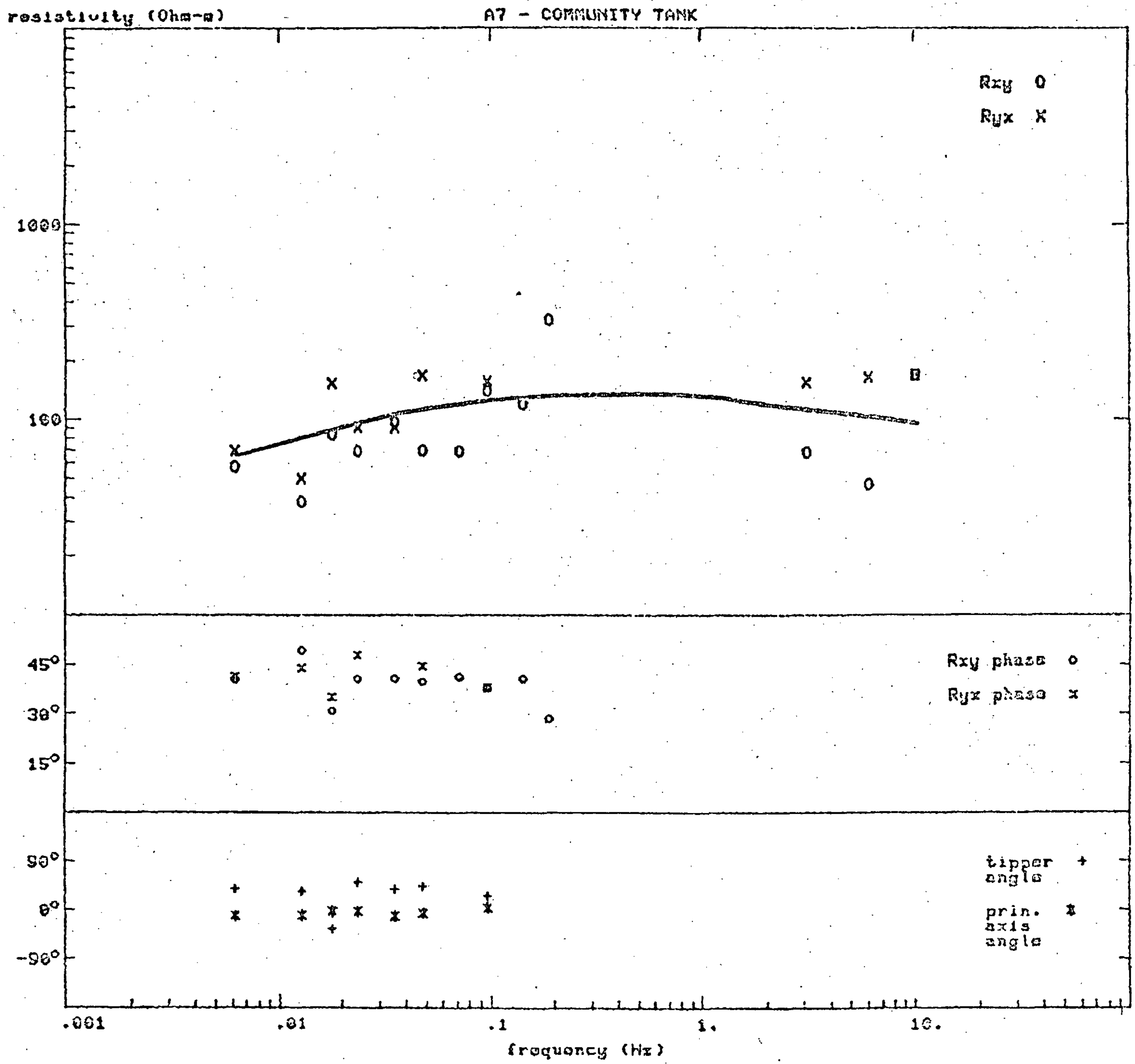
resistivity (Ohm-m)
A7 - COMMUNITY TANK
Rxy O
Ryx X
1000
100
Rxy phase o
Ryx phase x
45°
30°
15°
90°
0°
-90°
tipper angle +
prin. axis angle
.001
.01
.1
1.
10.
frequency (Hz)

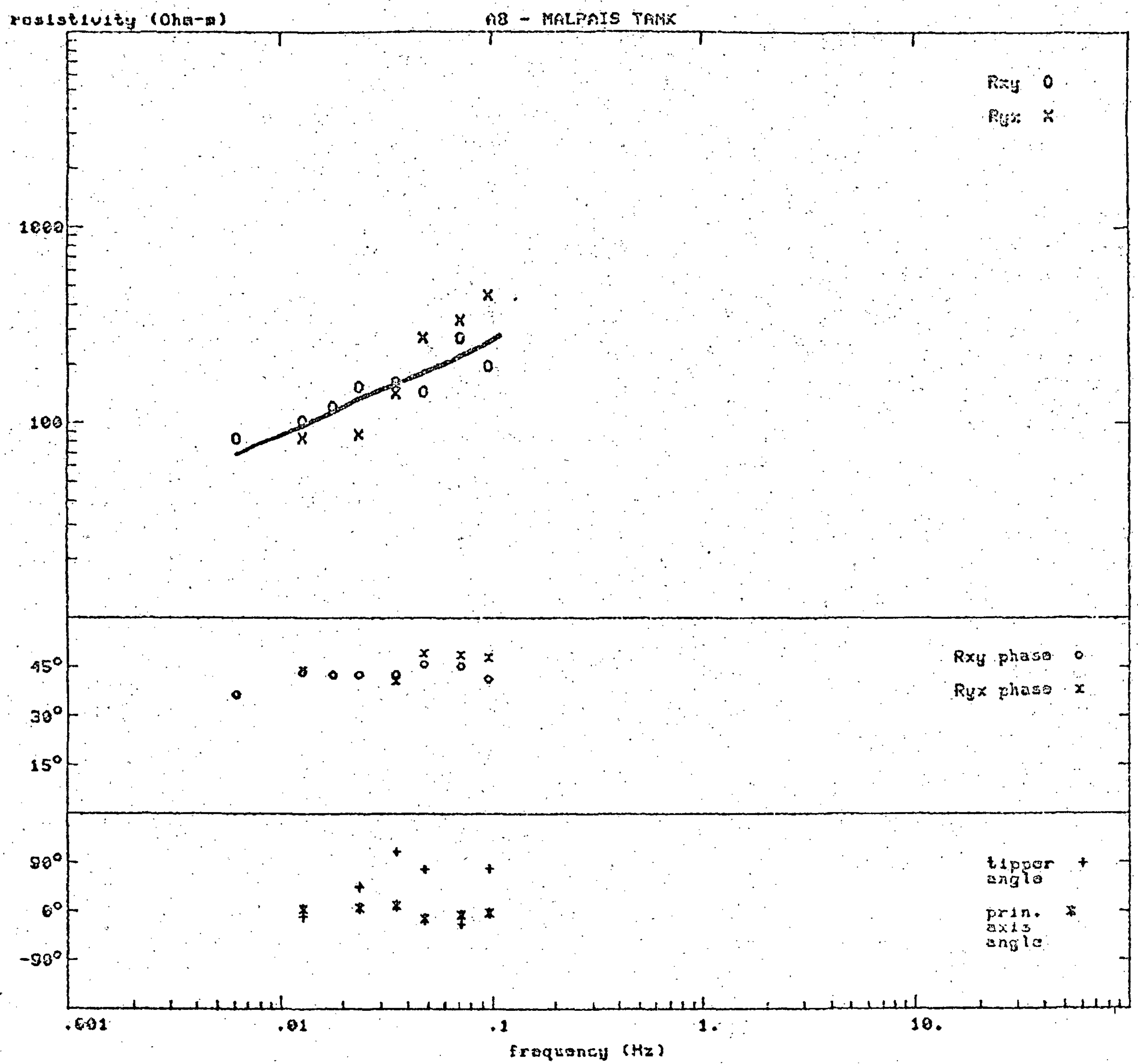
resistivity (Ohm-m)
A8 - MALPAIS TANK
Rxy O
Ryx X
1000
100
45°
30°
15°
Rxy phase o
Ryx phase x
90°
0°
-90°
tipper angle +
prin. axis angle
.001
.01
.1
1.
10.
frequency (Hz)

16

8

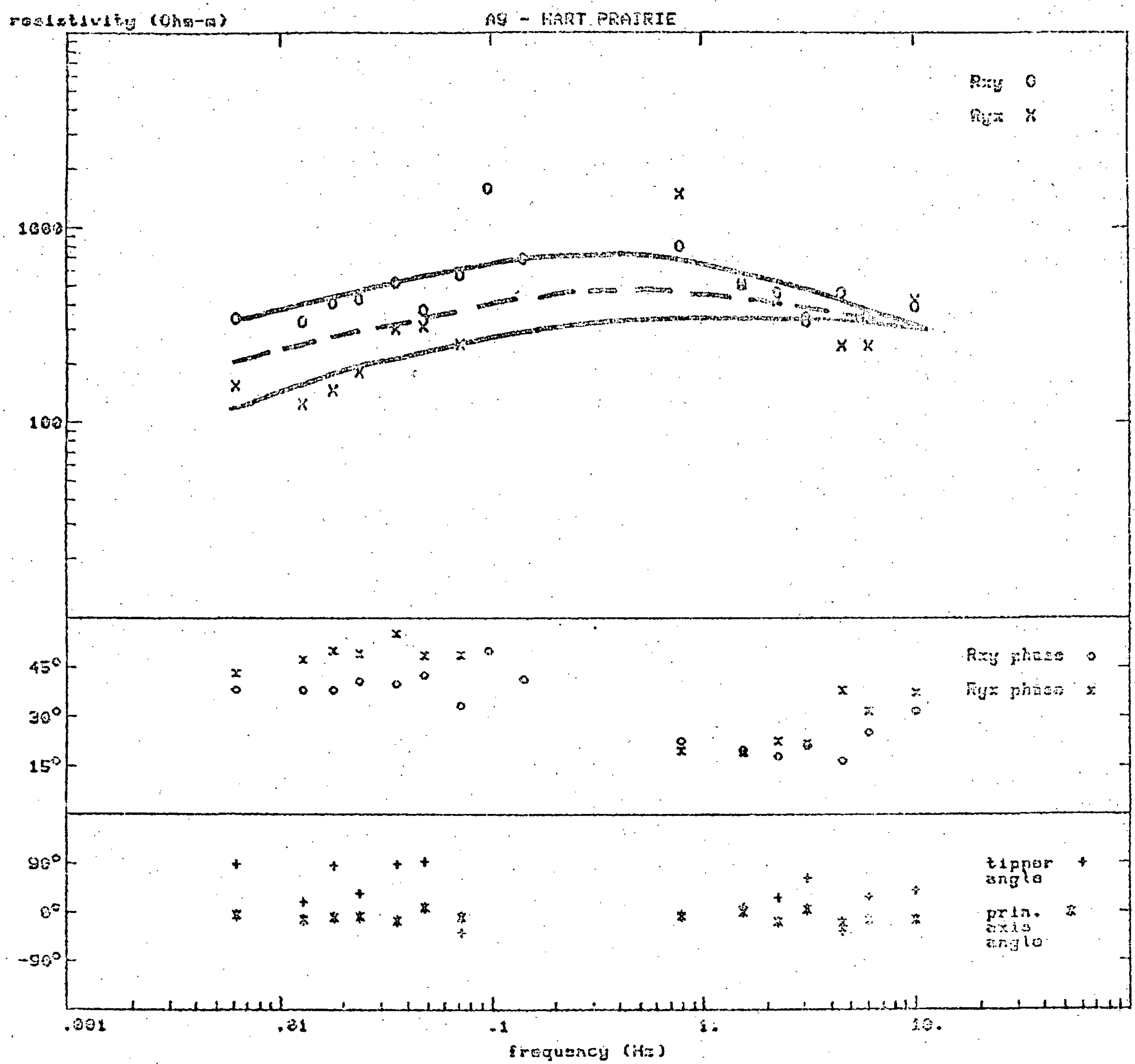
A9 - HART PRAIRIE
resistivity (Ohm-m)
Rxy O
Ryx X
1000
100
Rxy phase o
Ryx phase x
45°
30°
15°
tipper angle +
prin. axis angle
90°
0°
-90°
.001
.01
.1
1.
10.
frequency (Hz)

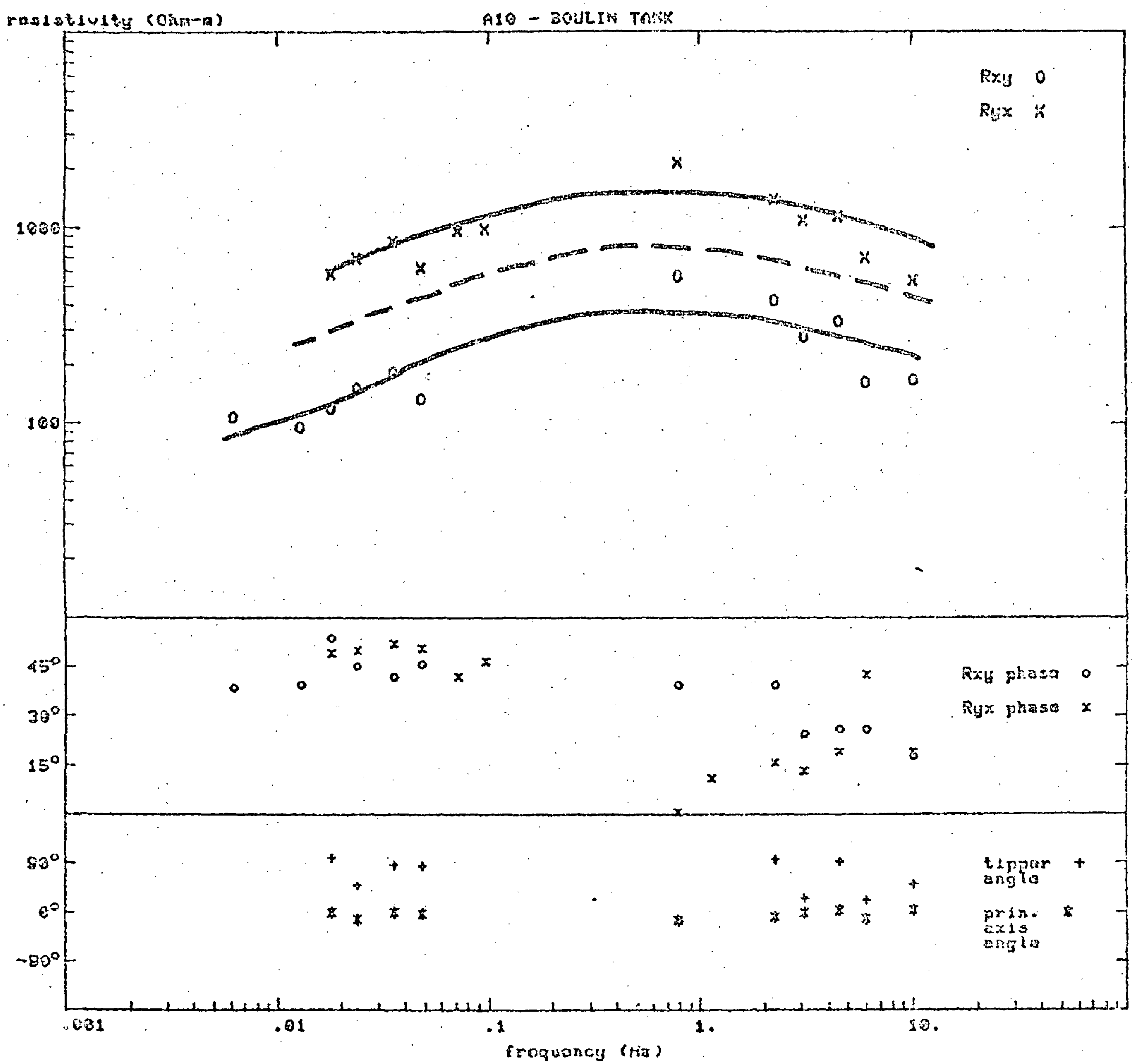

resistivity (Ohm-m)
A10 - BOULIN TANK
Rxy O
Ryx X
1000
100
Rxy phase o
Ryx phase x
45°
30°
15°
tipper angle +
prin. axis angle
90°
0°
-90°
.001
.01
.1
1.
10.
frequency (Hz)

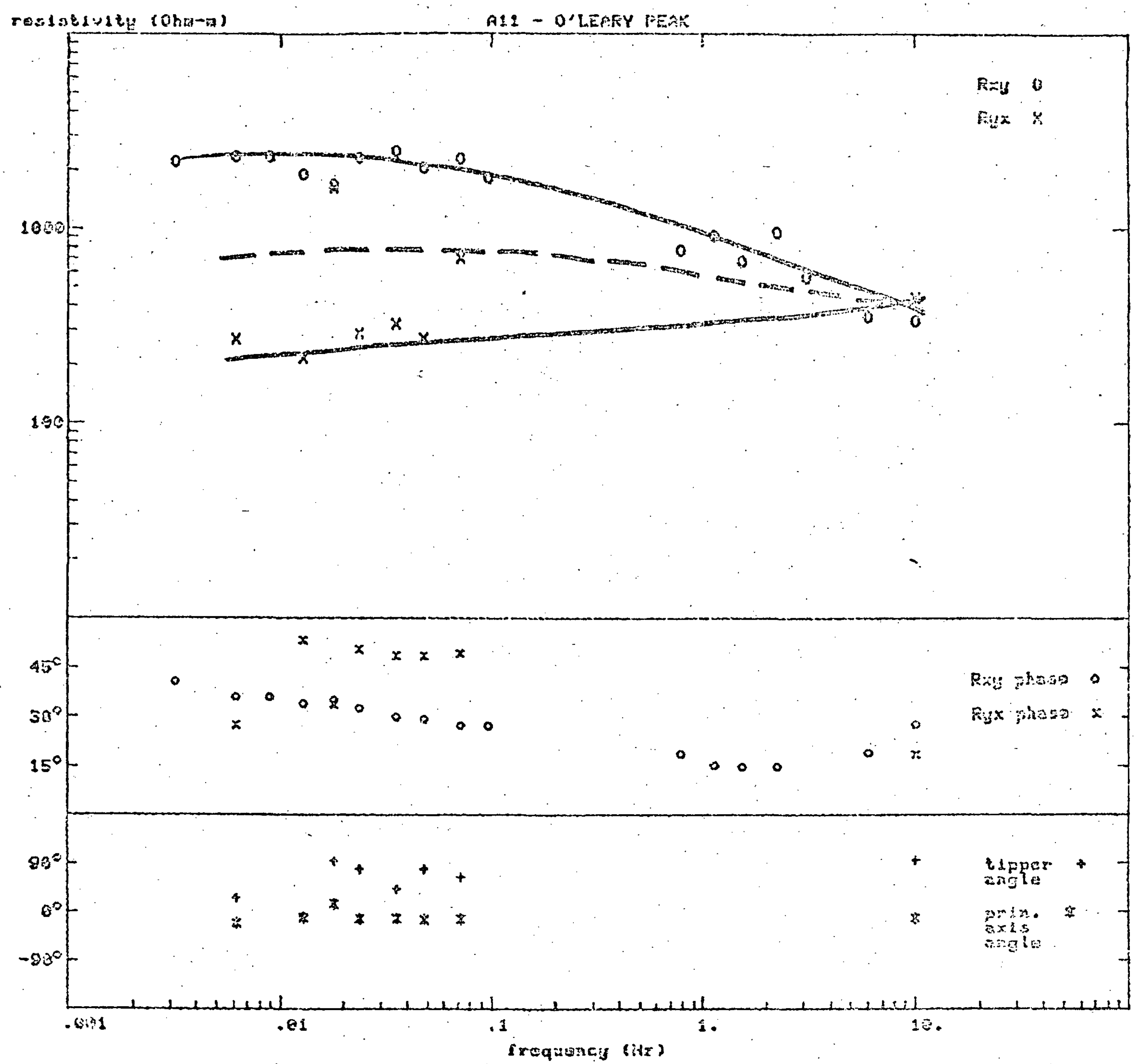
resistivity (Ohm-m)
A11 - O'LEARY PEAK
Rxy O
Ryx X
1000
100
45°
30°
15°
Rxy phase o
Ryx phase x
90°
0°
-90°
tipper angle +
prin. axis angle
.001
.01
.1
1.
10.
frequency (Hz)

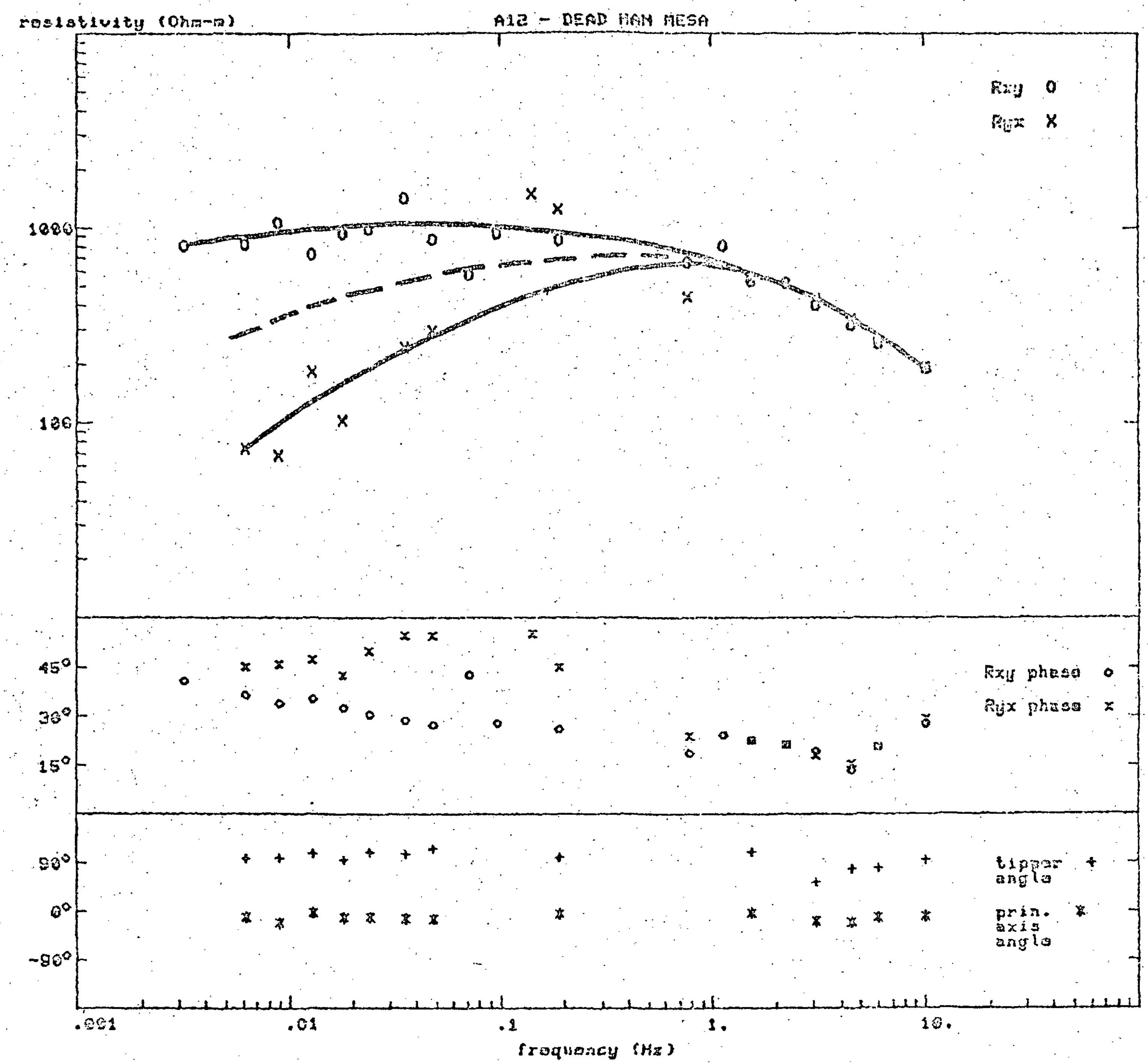

resistivity (Ohm-m)
A12 - DEAD MAN MESA
Rxy O
Ryx X
1000
100
45°
30°
15°
Rxy phase o
Ryx phase x
90°
0°
-90°
tipper angle +
prin. axis angle
.001
.01
.1
1.
10.
frequency (Hz)

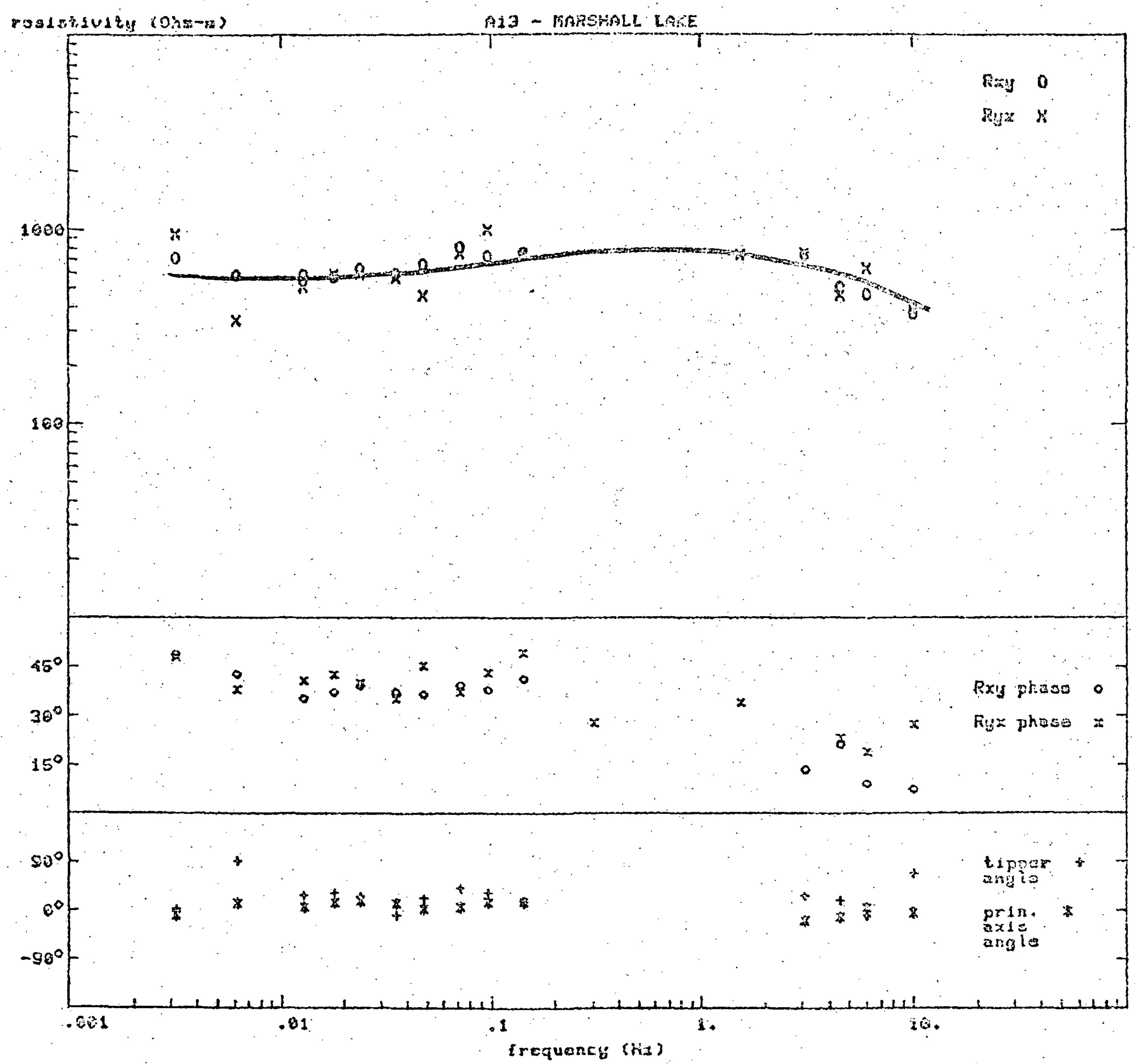

resistivity (Ohm-m)
A13 - MARSHALL LAKE
Rxy O
Ryx X
1000
100
45°
30°
15°
Rxy phase o
Ryx phase x
90°
0°
-90°
tipper angle +
prin. axis angle
.001
.01
.1
1.
10.
frequency (Hz)

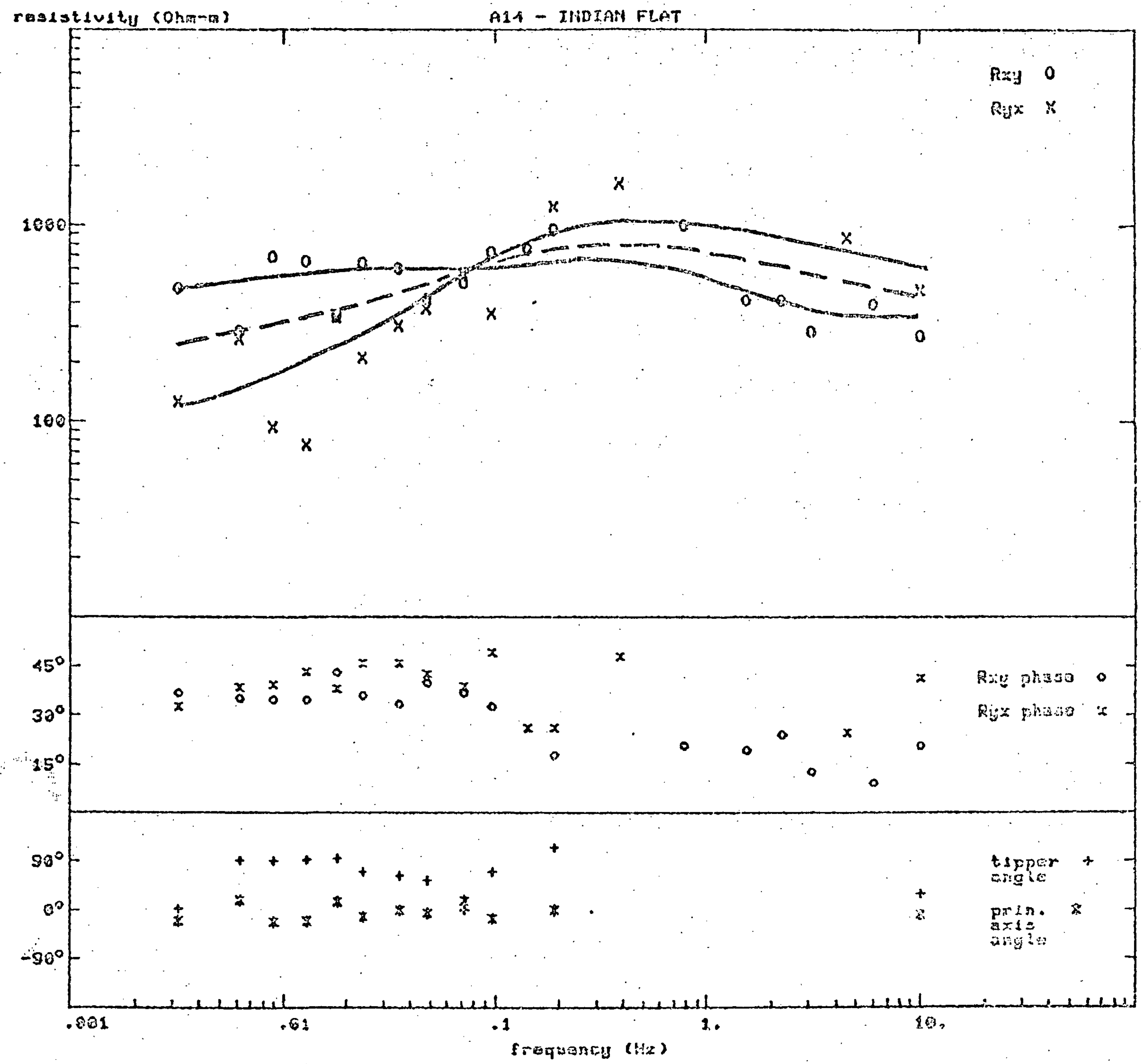

resistivity (Ohm-m)
A14 - INDIAN FLAT
Rxy O
Ryx X
1000
100
45°
30°
15°
Rxy phase o
Ryx phase x
90°
0°
-90°
tipper angle +
prin. axis angle
.001
.01
.1
1.
10.
frequency (Hz)

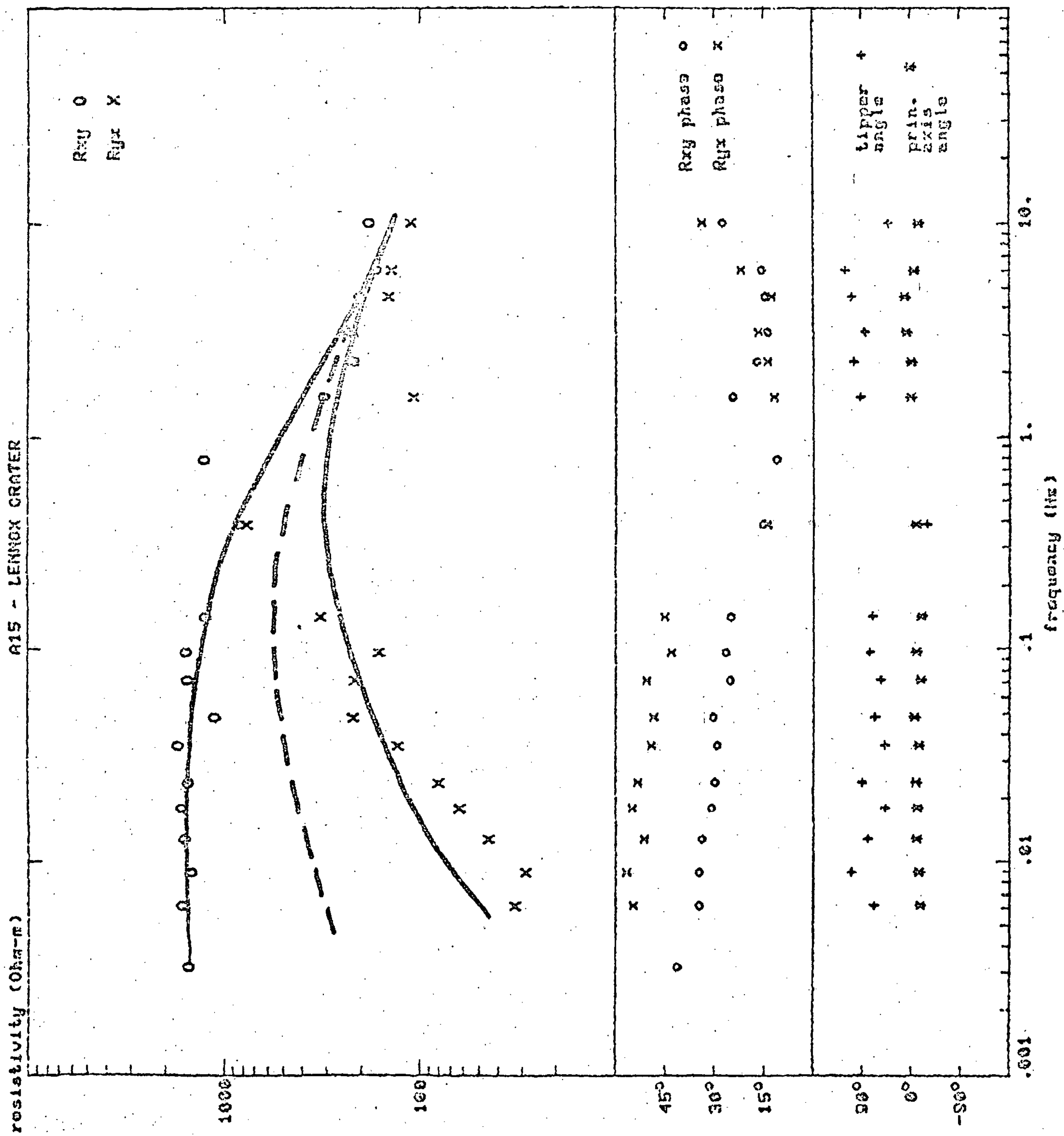
A15 - LENNOX CRATER
resistivity (Ohm-m)
1000
100
Rxy O
Ryx X
Rxy phase o
Ryx phase x
45°
30°
15°
tipper angle +
prin-axis angle *
90°
0°
-90°
.001
.01
.1
1.
10.
frequency (Hz)

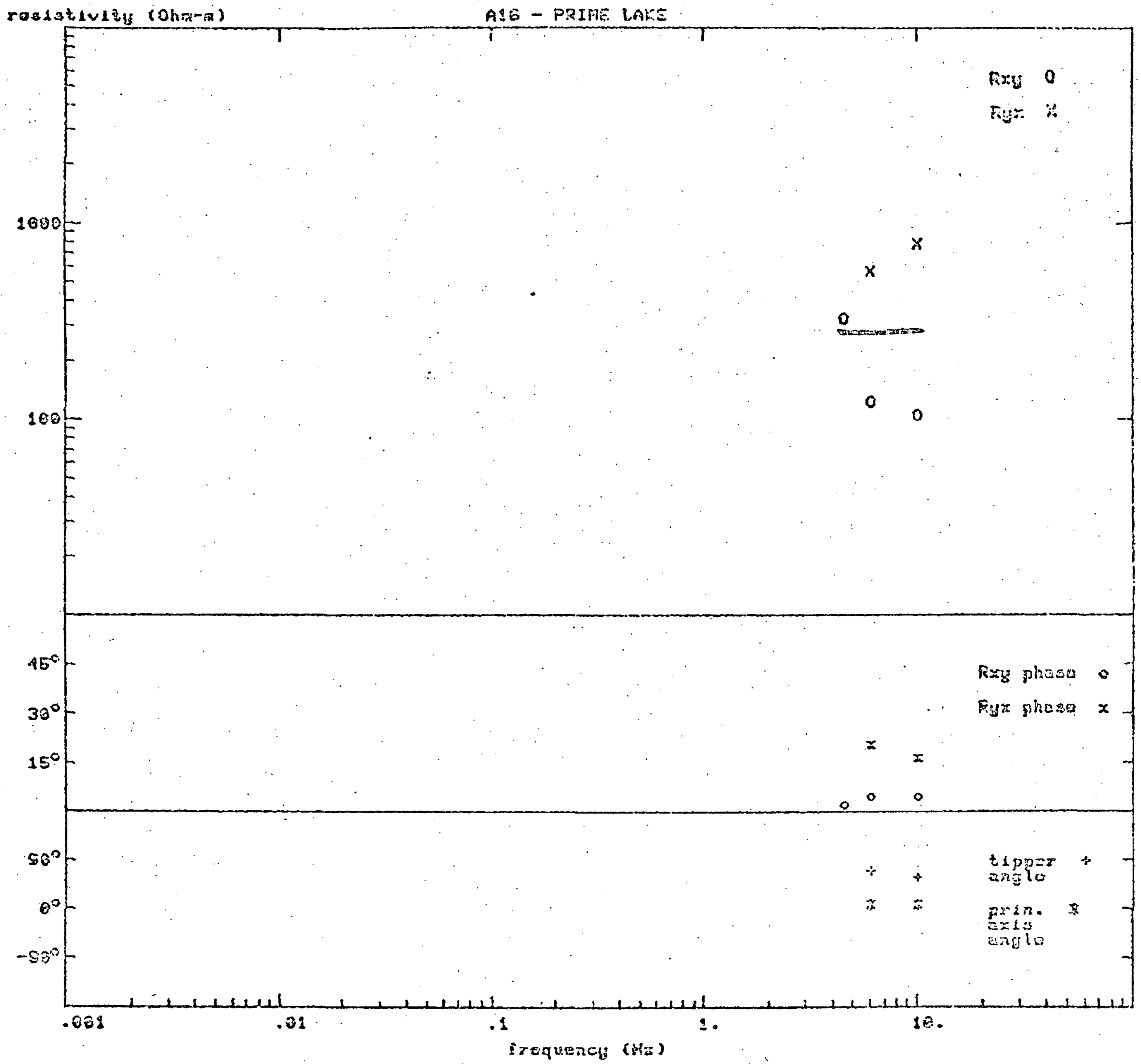
resistivity (Ohm-m)
A16 - PRIME LAKE
Rxy O
Ryx X
1000
100
45°
30°
15°
90°
0°
-90°
Rxy phase o
Ryx phase x
tipper angle +
prin. axis angle $
.001
.01
.1
1.
10.
frequency (Hz)

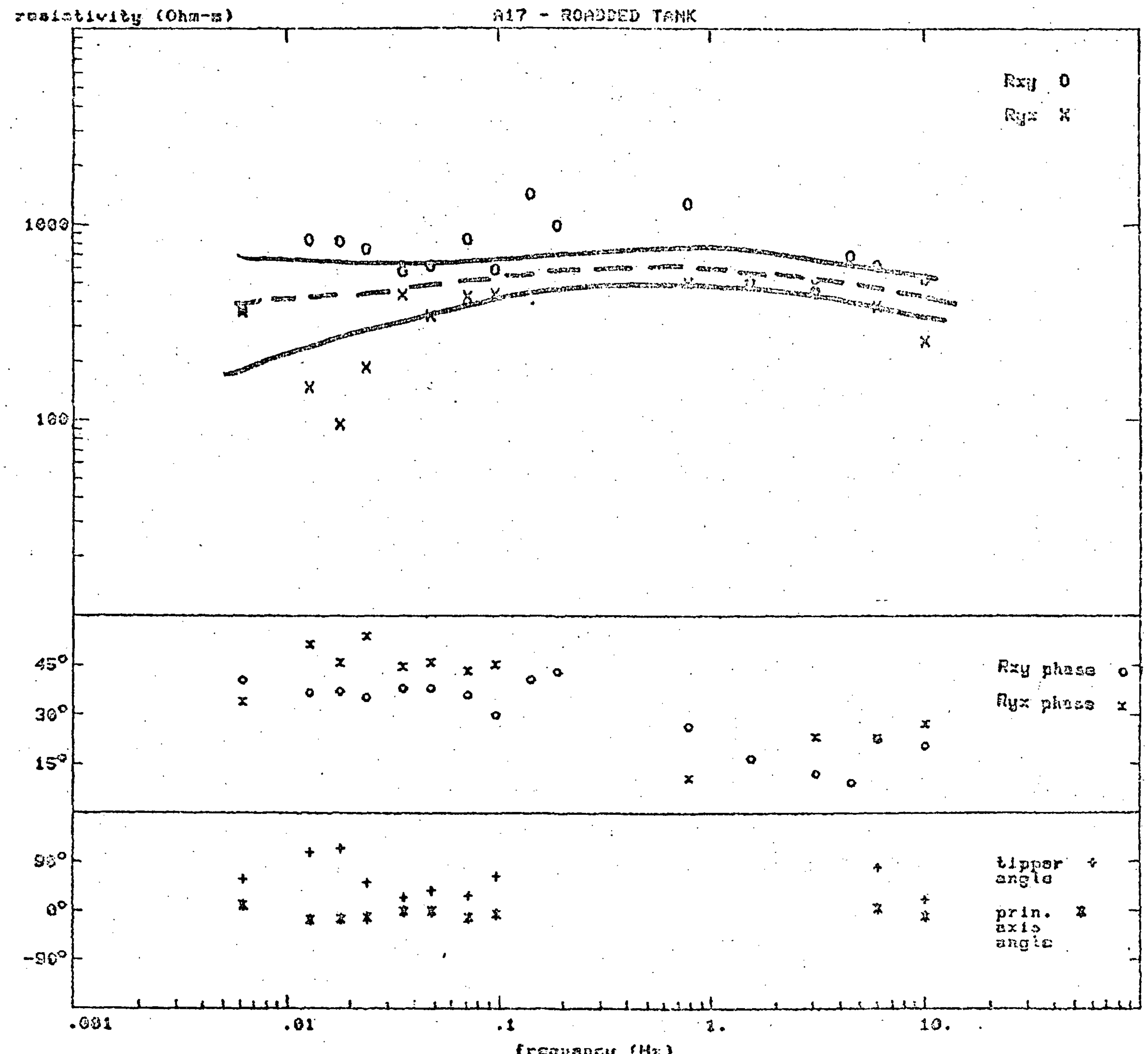

resistivity (Ohm-m)
A17 - ROADDED TANK
Rxy O
Ryx X
1000
100
45°
30°
15°
Rxy phase o
Ryx phase x
90°
0°
-90°
tipper angle +
prin. axis angle
.001
.01
.1
1.
10.
frequency (Hz)

A1-CINDER LAKE R1

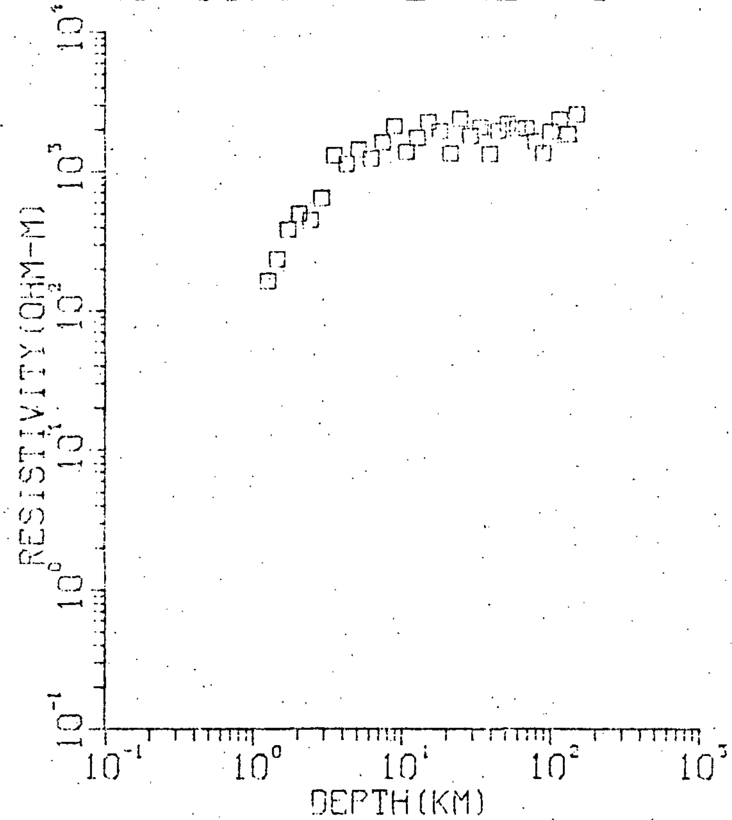

A1 CINDER LAKE R2

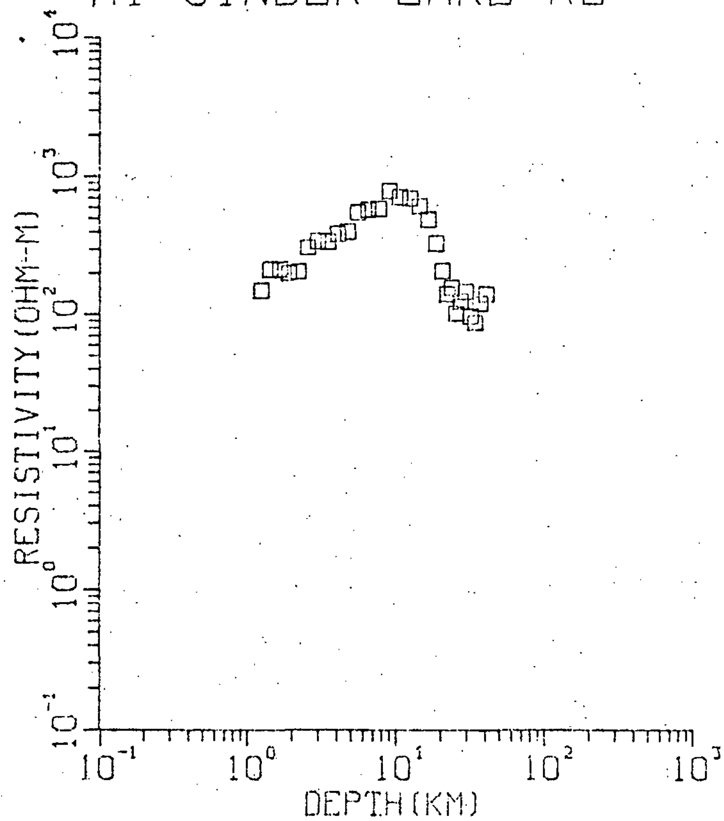

A1-CINDER LAKE R3

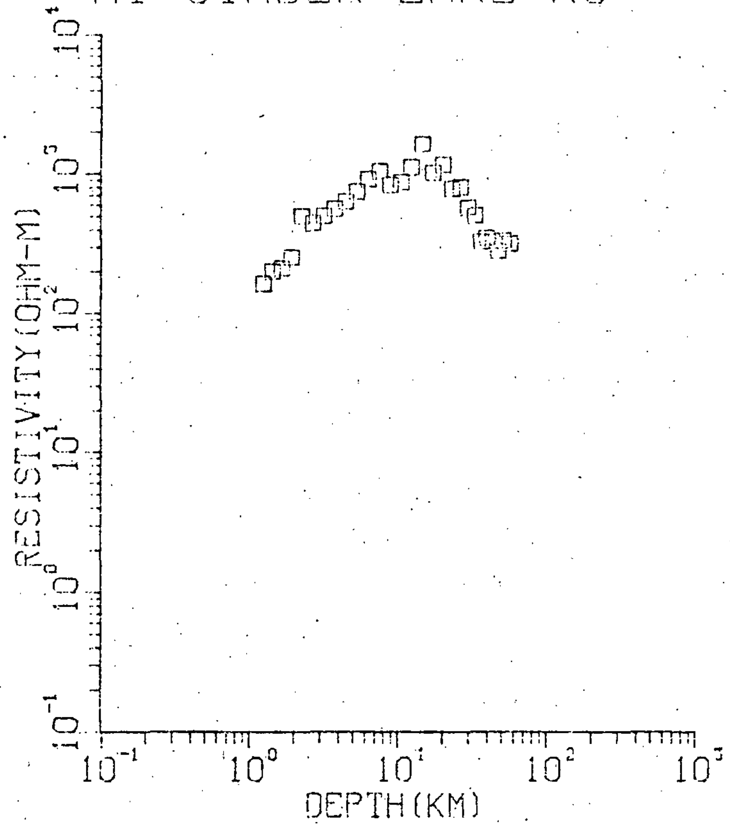

A2-WATER TANK R1

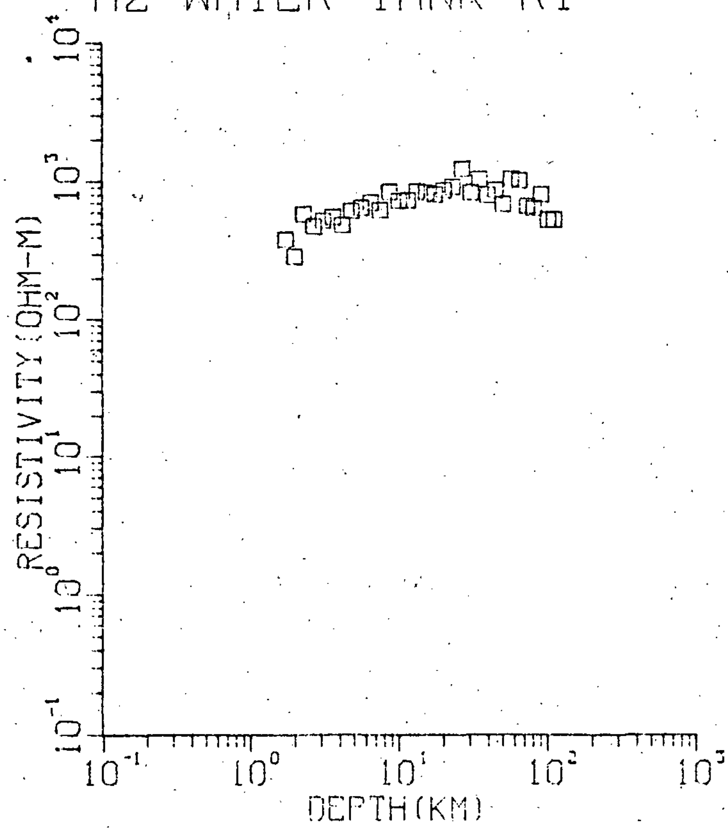

A4-DEAD MAN MESA R1

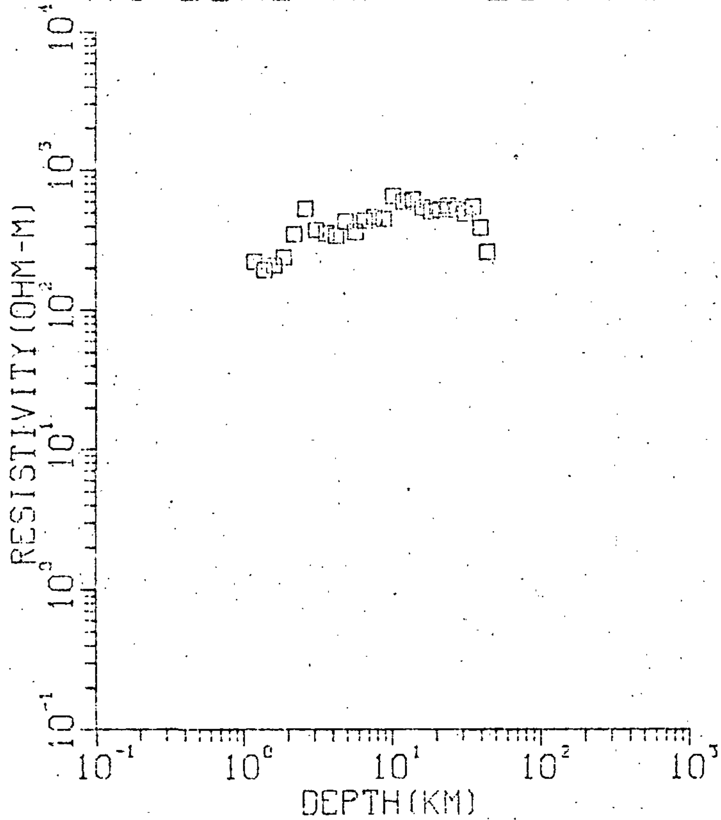

A5-KENDRICK PARK R1

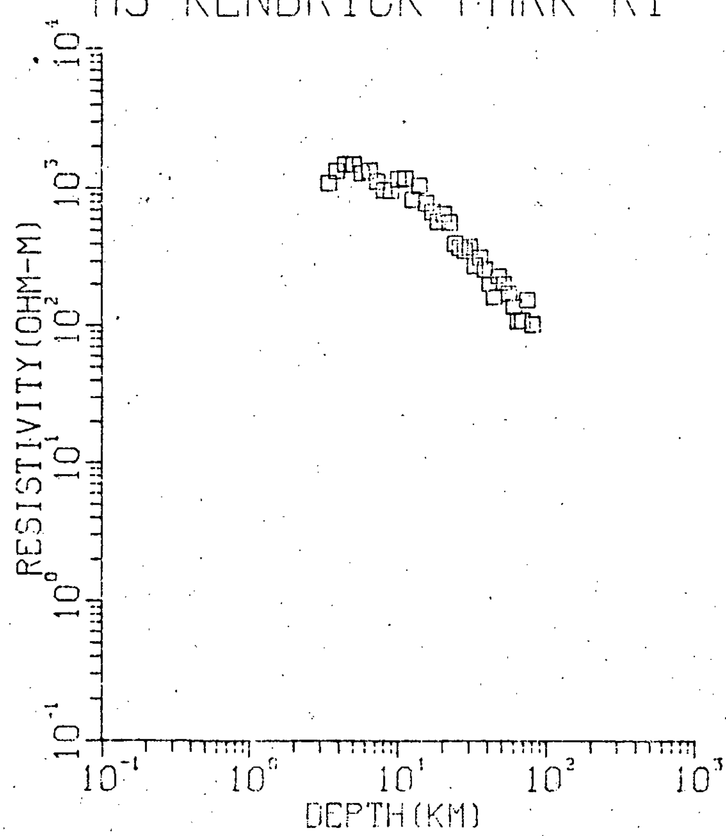

A6-LOCKETT MEADOW R1

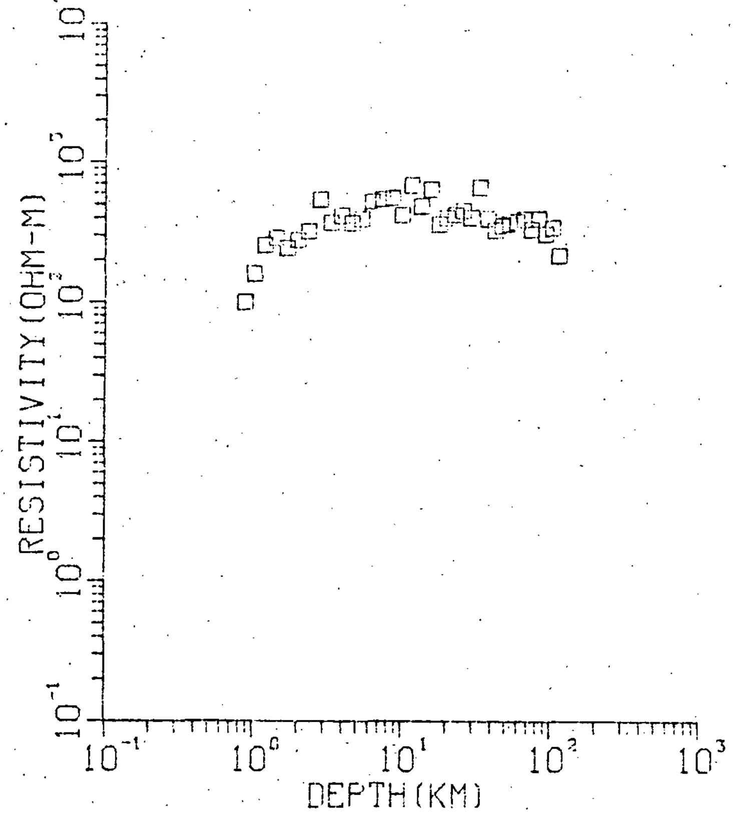

A6-LOCKETT MEADOW R2

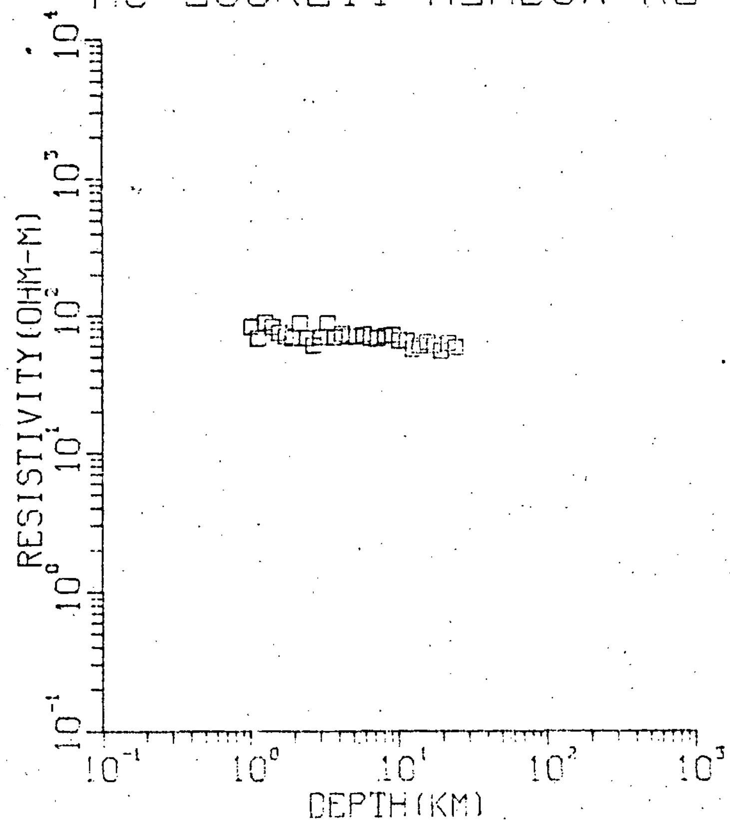

A6-LOCKETT MEADOW R3

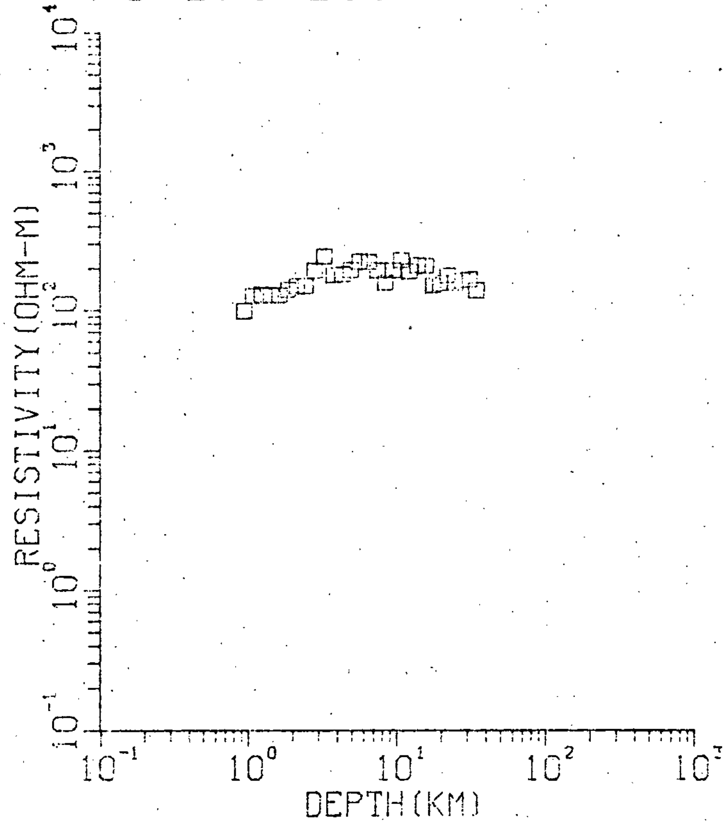

A7-COMMUNITY TANK R1

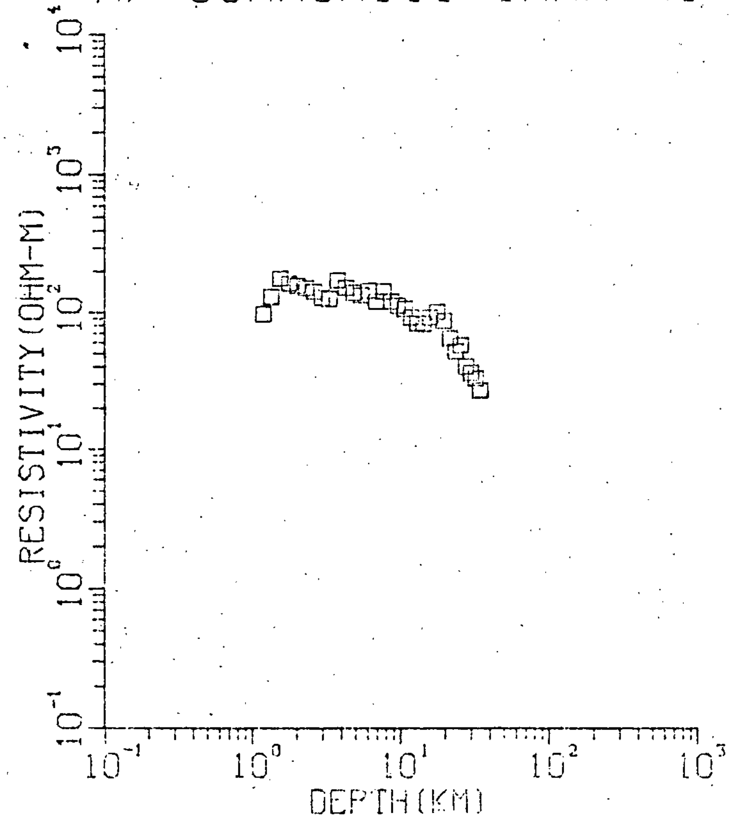

A9-HART PRAIRIE R1

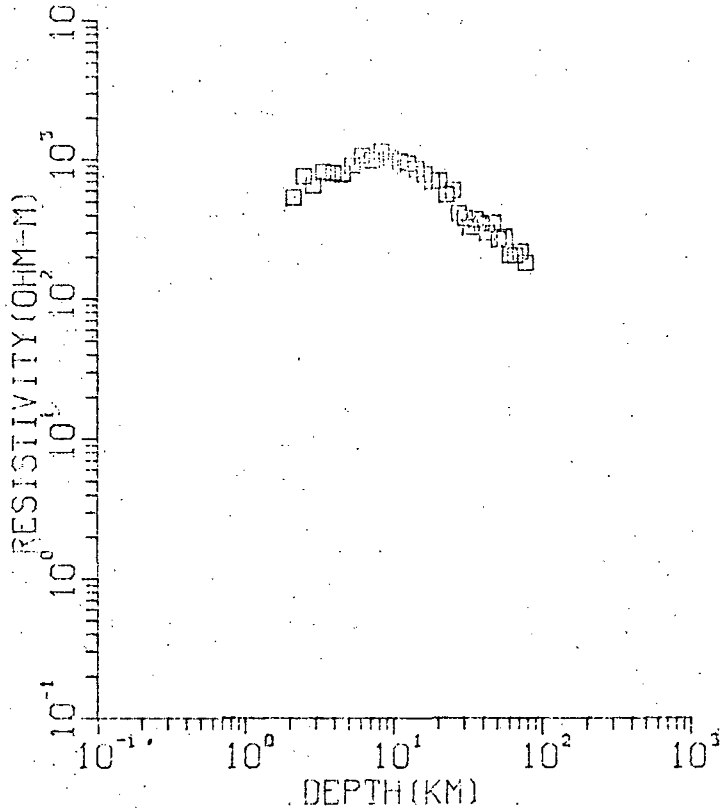

A9-HART PRAIRIE R2

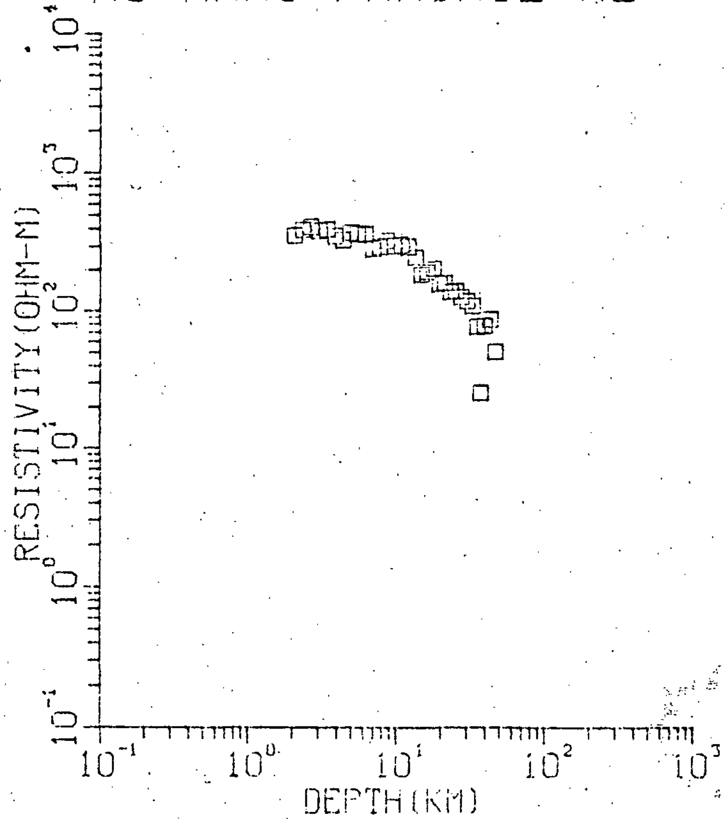

A9-HART PRAIRIE R3

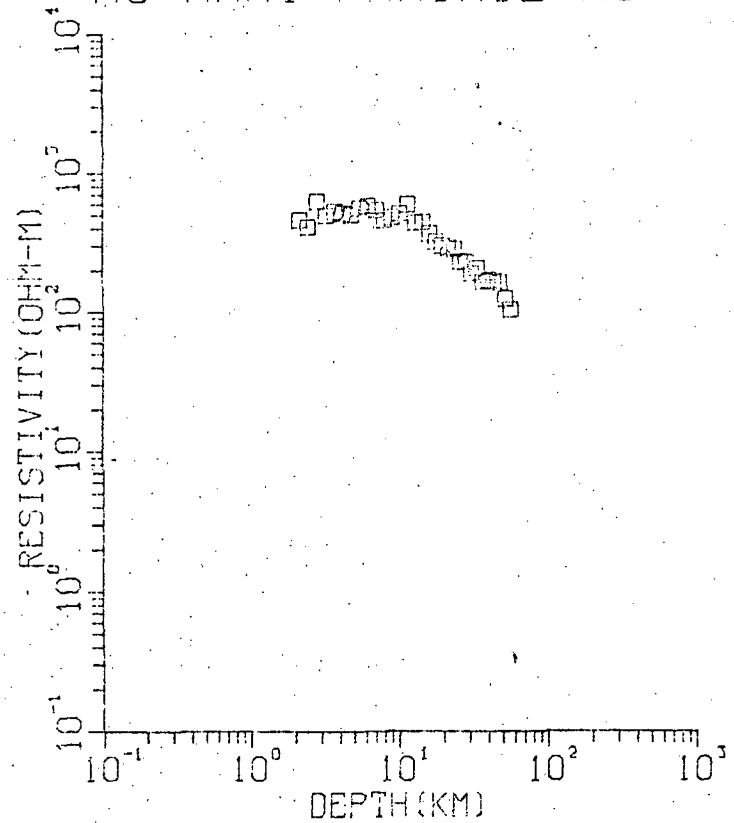

A10-BOULIN TANK R1

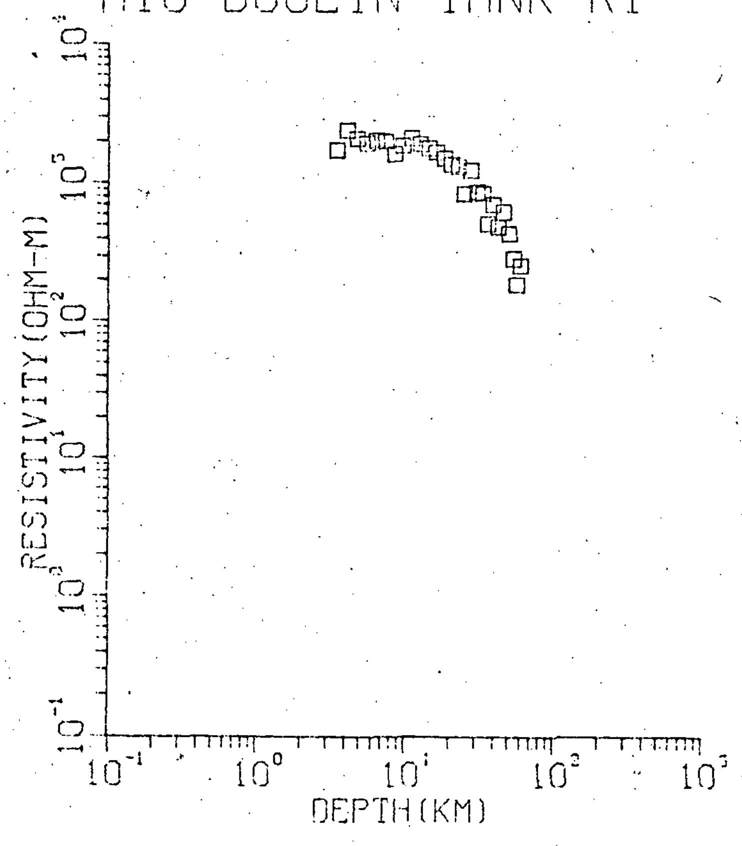

A10-BOULIN TANK R2

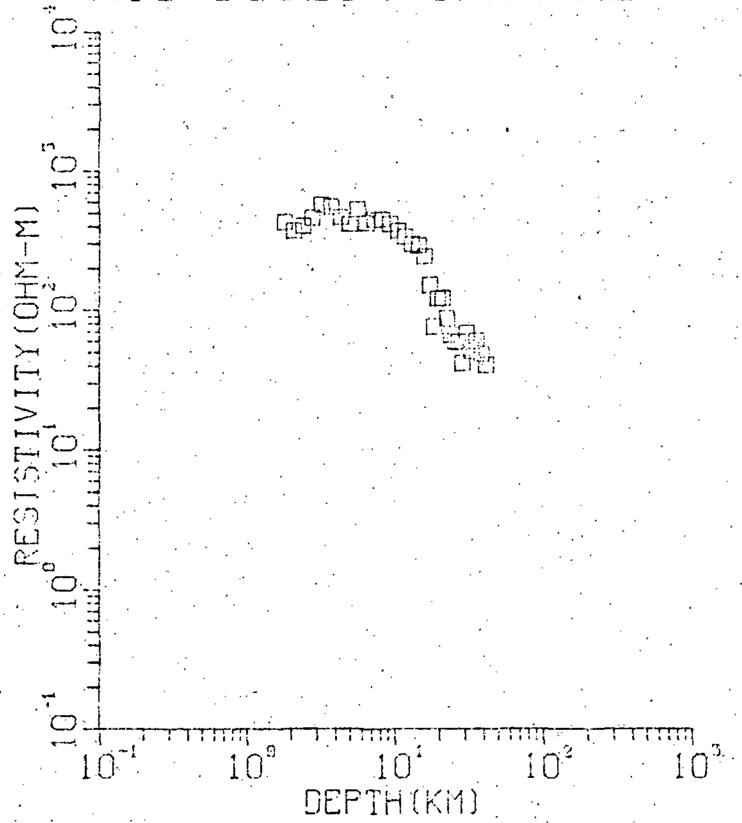

A10-BOULIN TANK R3

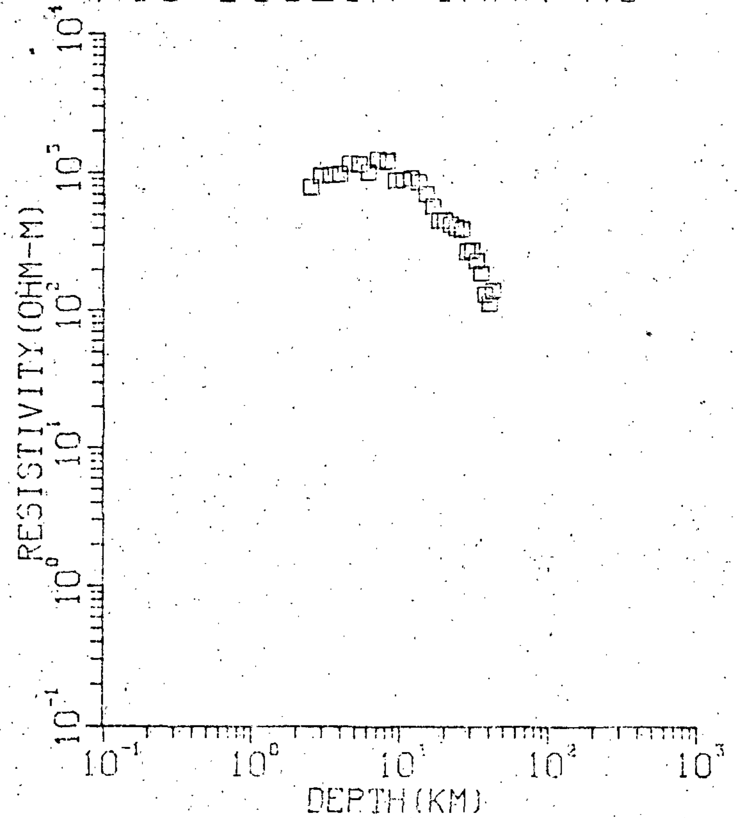

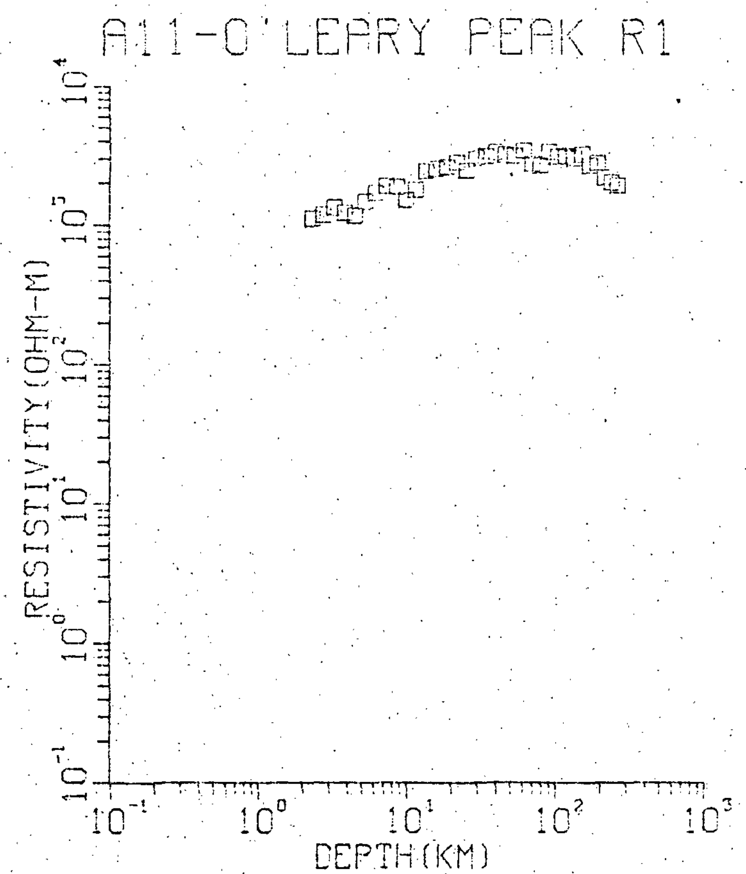
A11-O'LEARY PEAK R1
RESISTIVITY(OHM-M)
10^{-1}
10^{0}
10^{1}
10^{2}
10^{3}
10^{4}
DEPTH(KM)

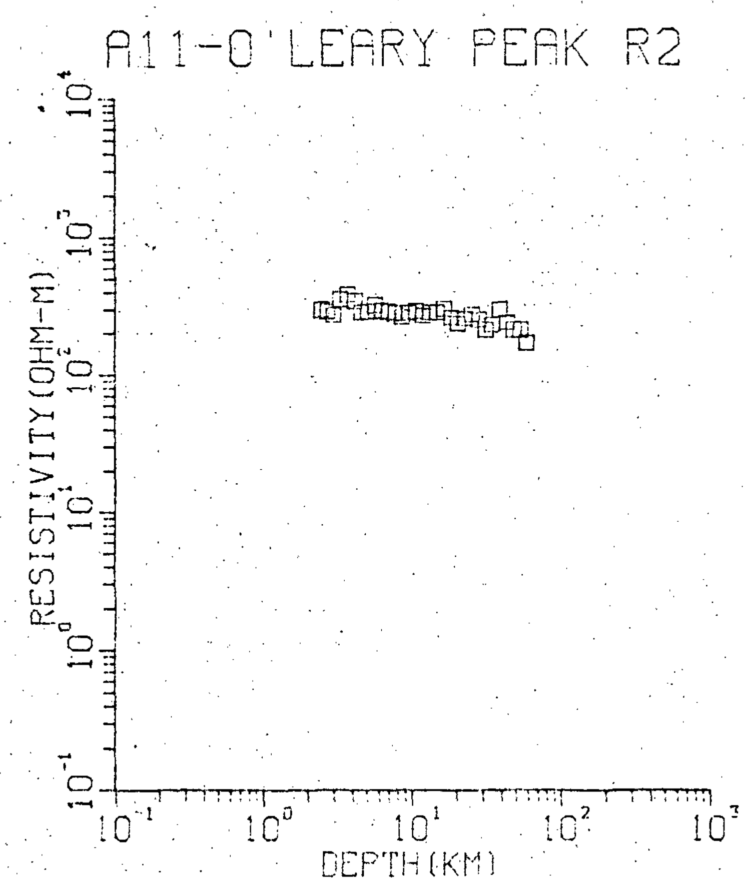
A11-O'LEARY PEAK R2
RESISTIVITY(OHM-M)
10^{-1}
10^{0}
10^{1}
10^{2}
10^{3}
10^{4}
DEPTH(KM)

A11-O'LEARY PEAK R3

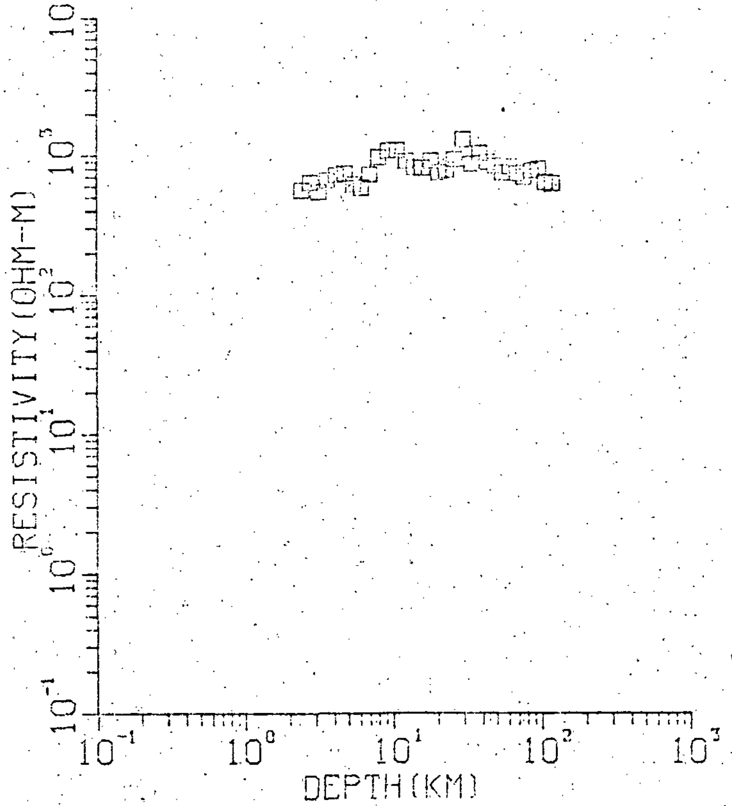

A12-DEAD MAN MESA R1

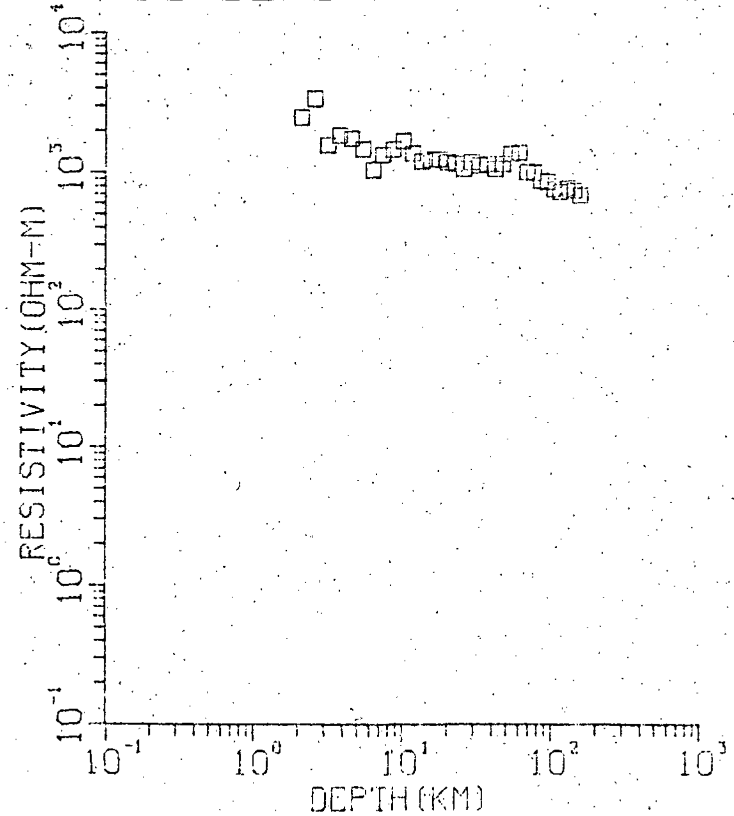

A12-DEAD MAN MESA R2

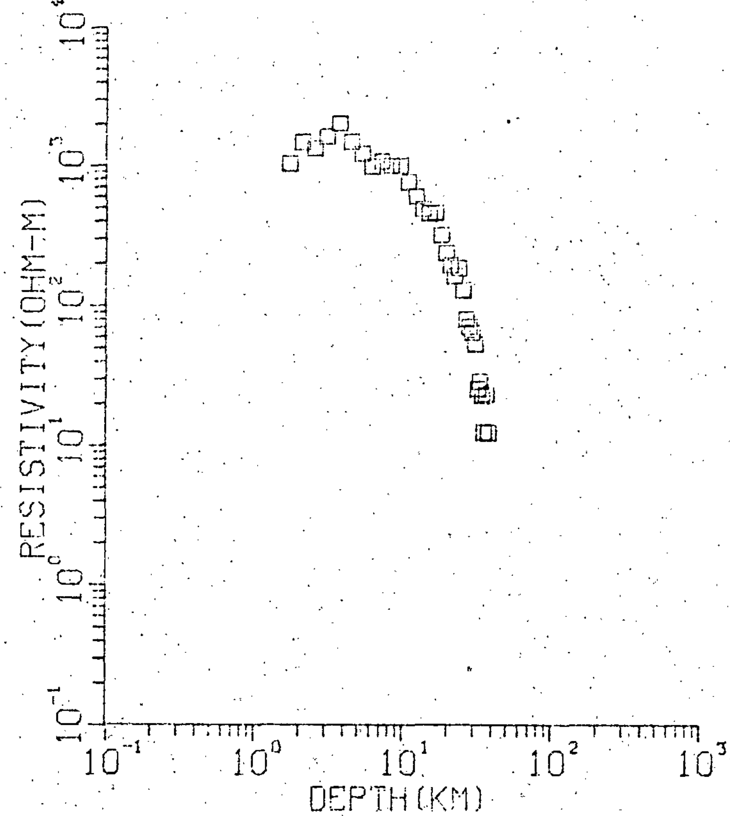

A12-DEAD MAN MESA R3

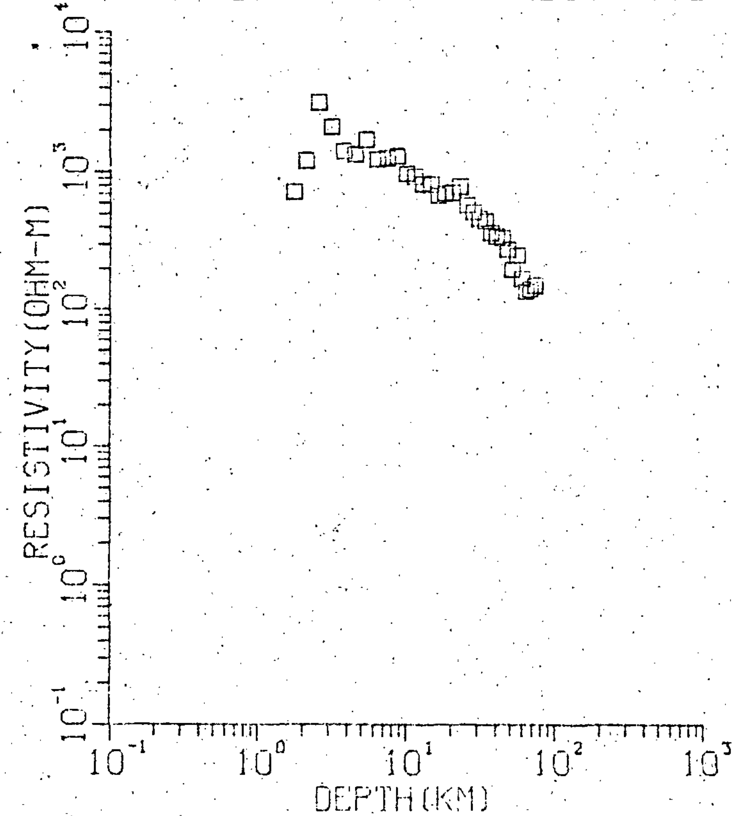

A~~10~~13-MARSHALL LAKE R1

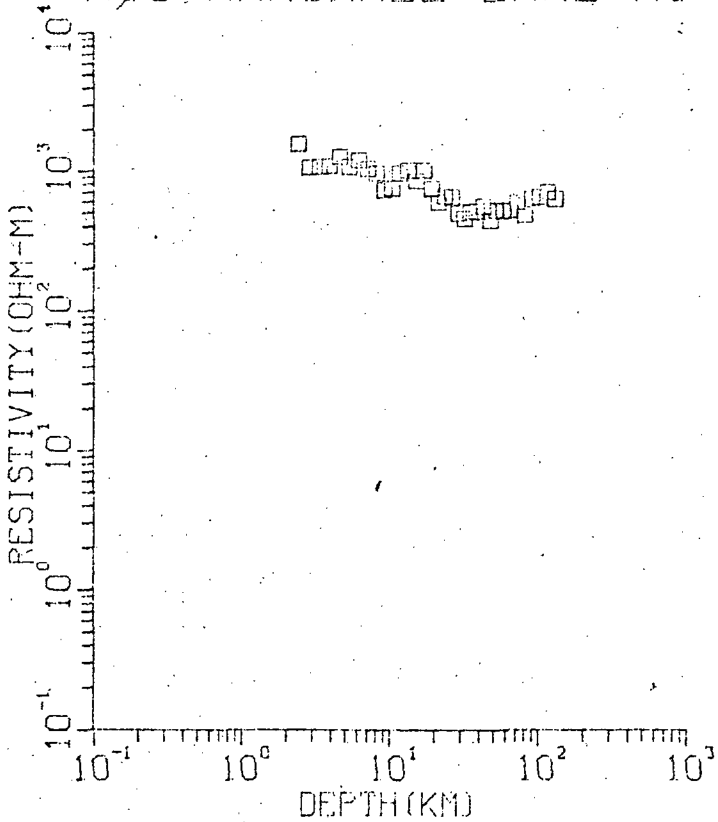

A14-INDIAN FLAT R1

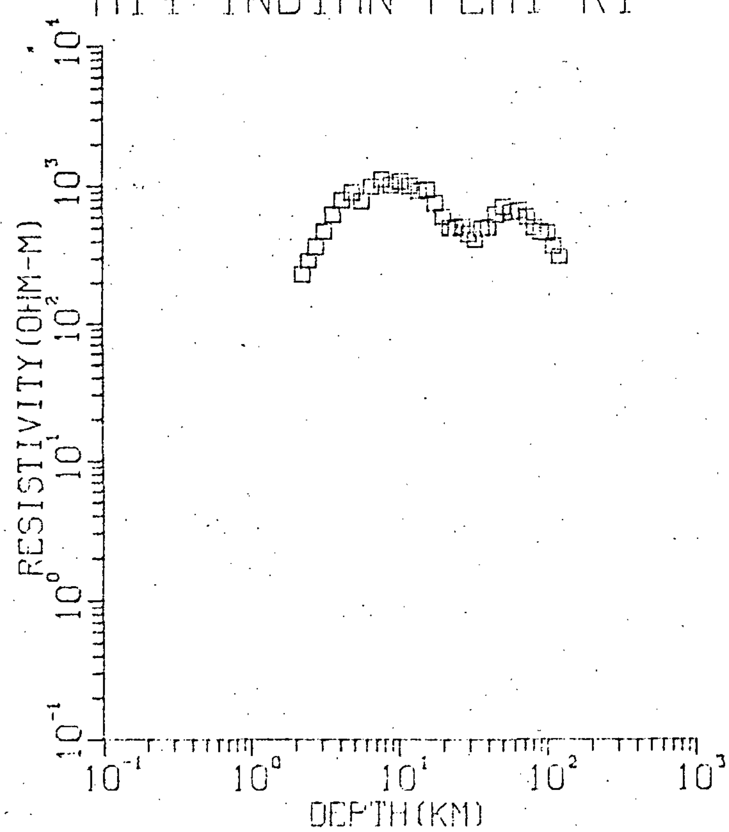

A14-INDIAN FLAT R2

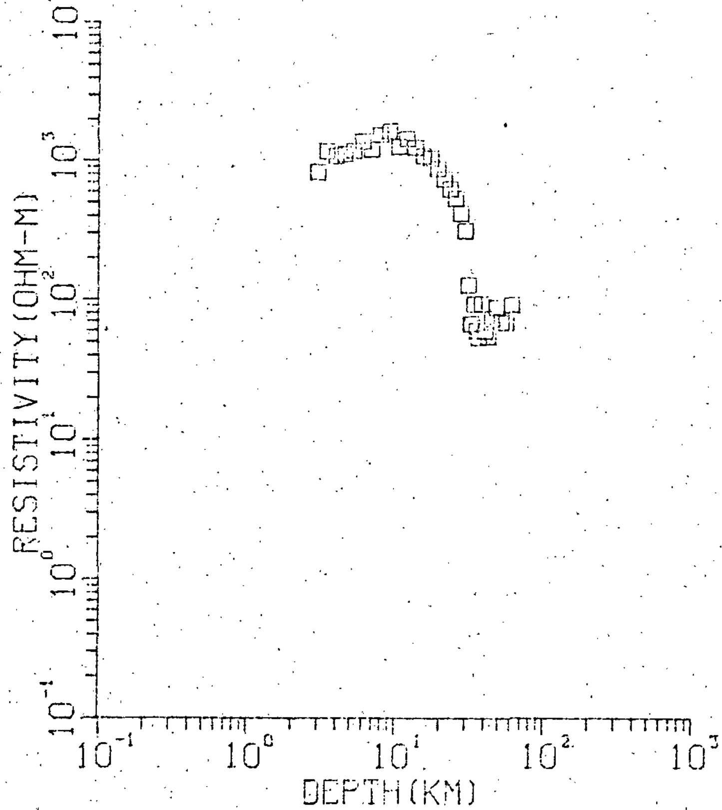

A14-INDIAN FLAT R3

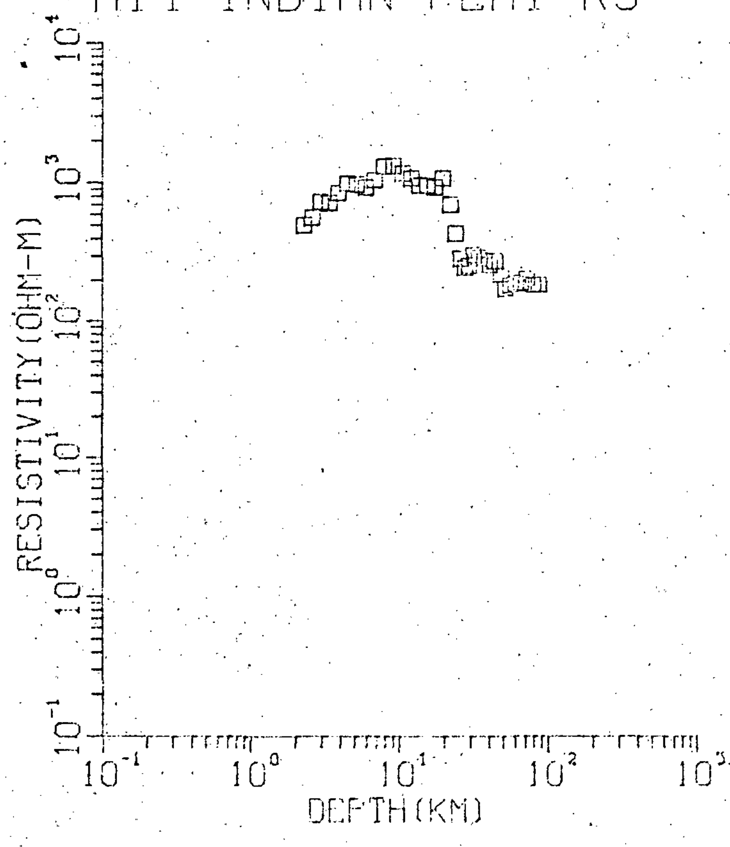

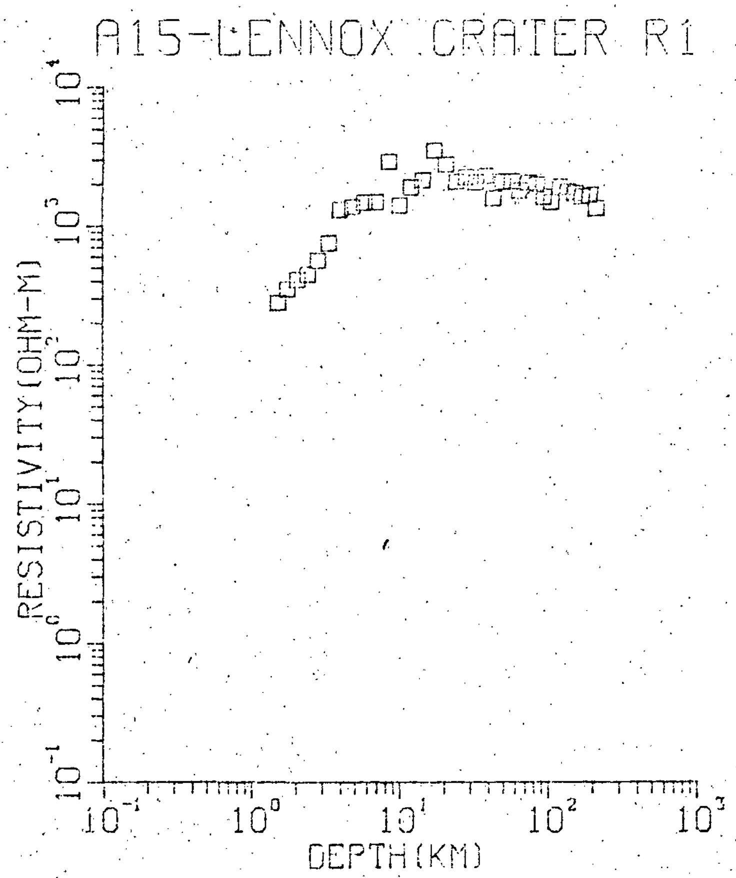
A15-LENNOX CRATER R1
RESISTIVITY(OHM-M)
DEPTH(KM)

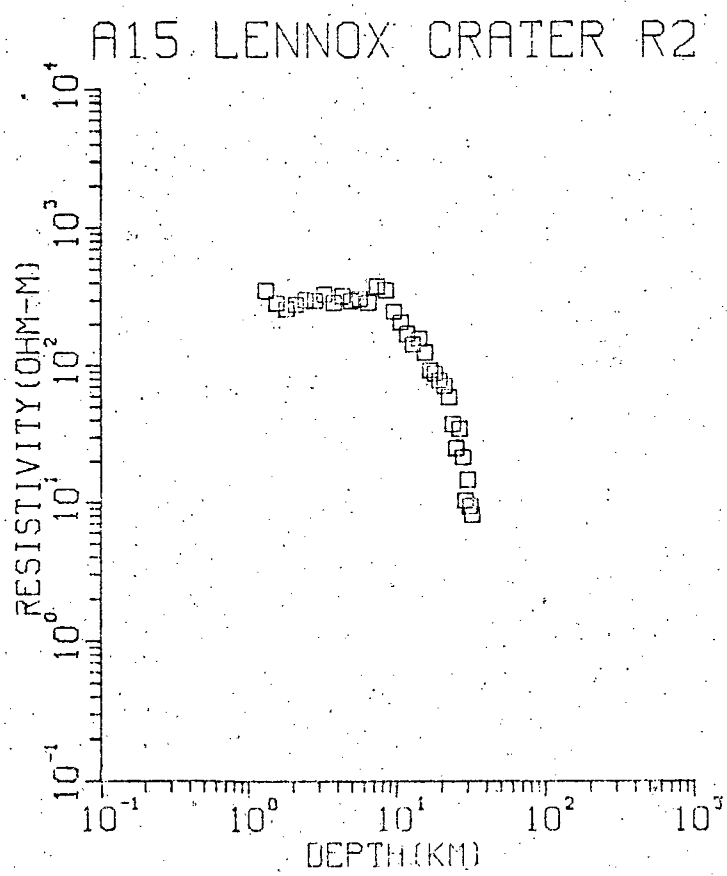
A15 LENNOX CRATER R2
RESISTIVITY(OHM-M)
DEPTH(KM)

A15-LENNOX CRATER R3

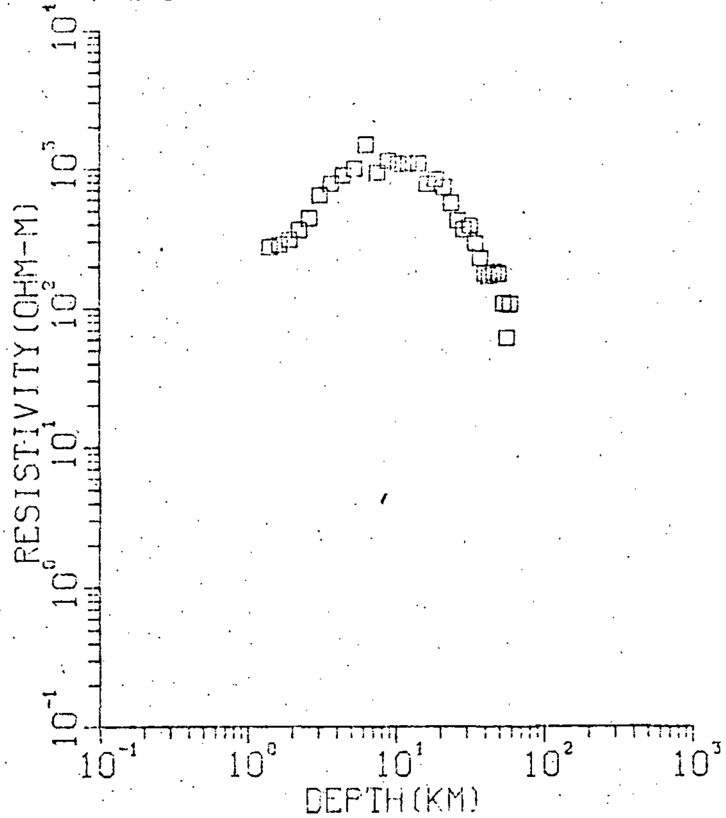

A17-ROADBED TANK R1

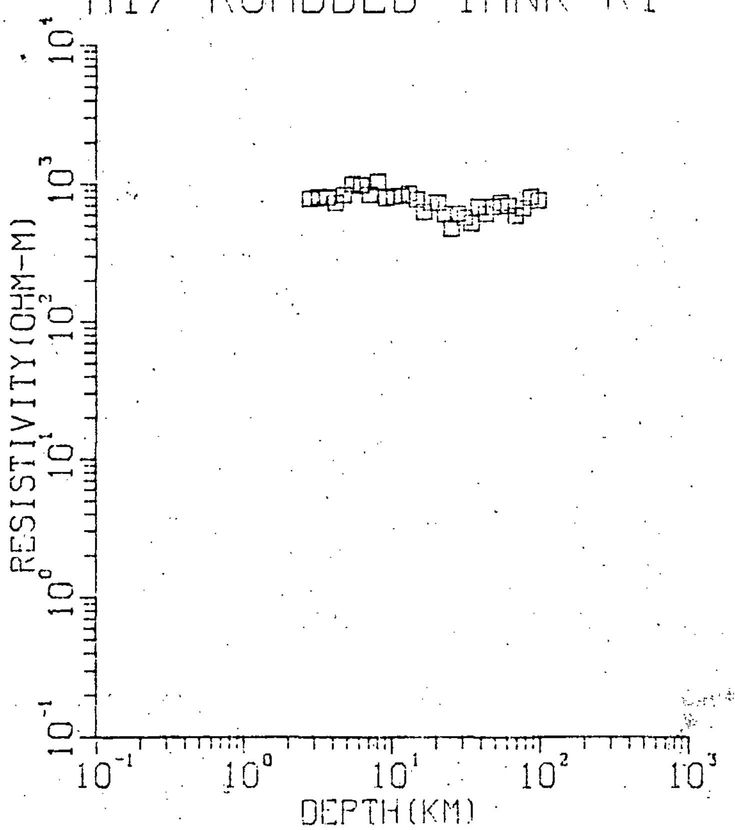

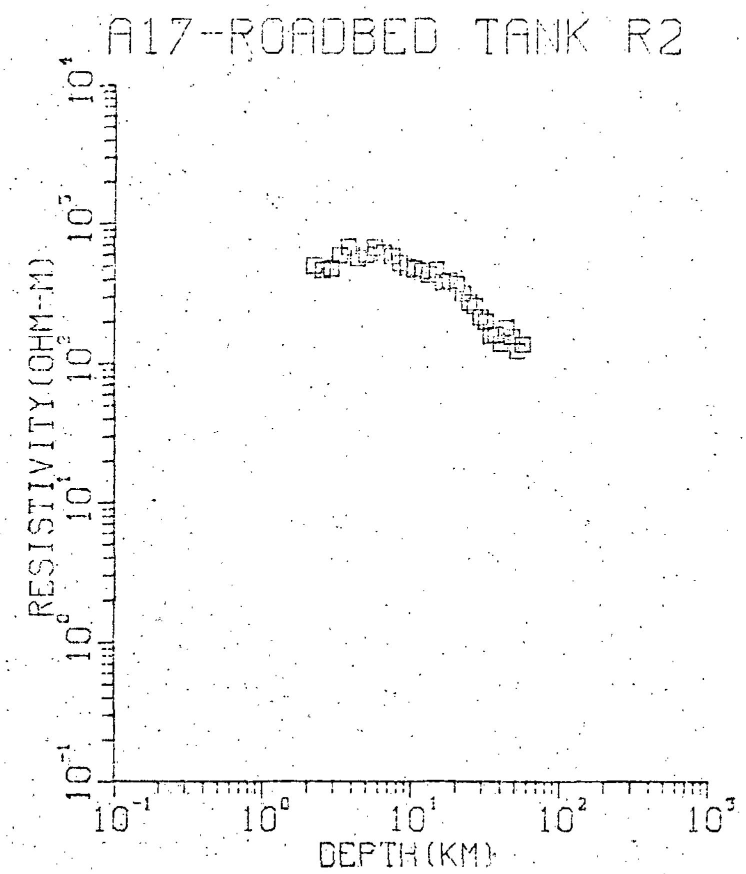
A17-ROADBED TANK R2
RESISTIVITY(OHM-M)
DEPTH(KM)

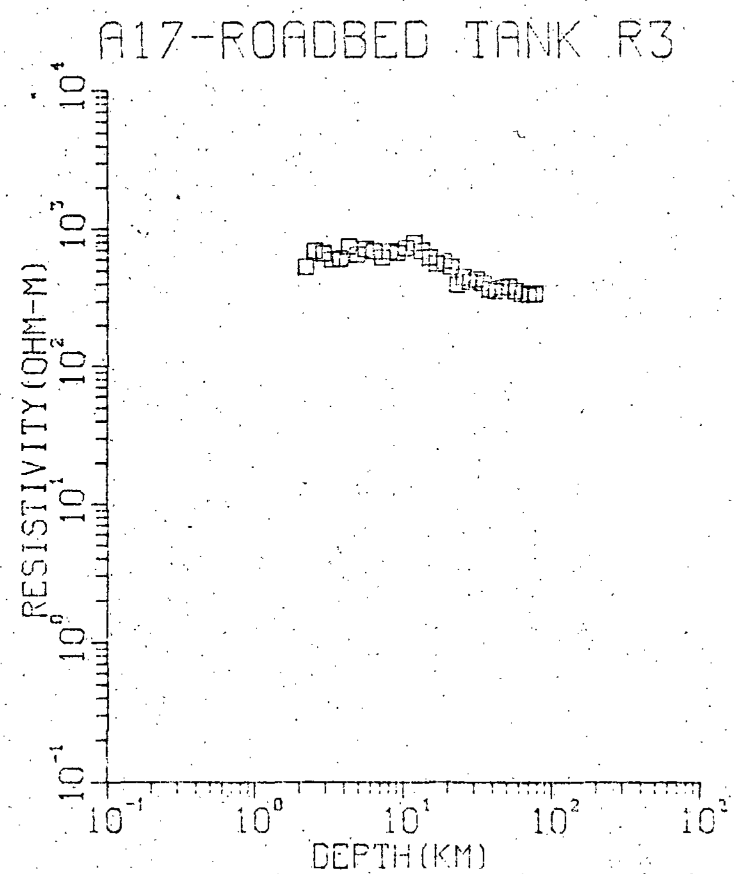
A17-ROADBED TANK R3
RESISTIVITY(OHM-M)
DEPTH(KM)

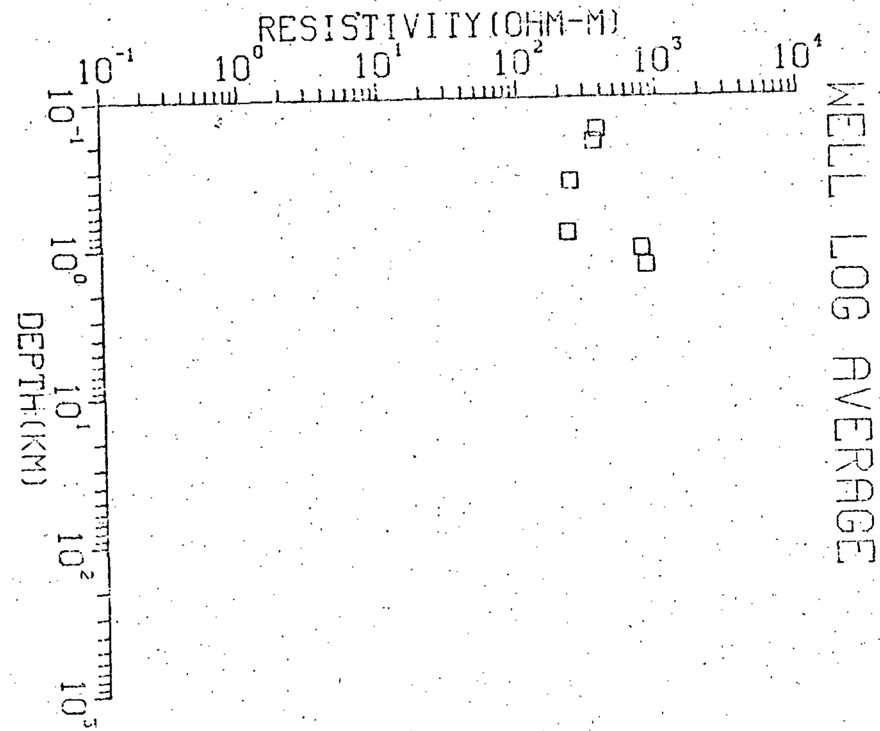
WELL LOG AVERAGE
RESISTIVITY(OHM-M)
DEPTH(KM)